



HAL
open science

The origin and dynamics of nitrogen in the Earth's mantle constrained by $^{15}\text{N}/^{14}\text{N}$ in hydrothermal gases

Jabrane Labidi, Edward Young

► To cite this version:

Jabrane Labidi, Edward Young. The origin and dynamics of nitrogen in the Earth's mantle constrained by $^{15}\text{N}/^{14}\text{N}$ in hydrothermal gases. *Chemical Geology*, 2022, 591, pp.120709. <10.1016/j.chemgeo.2022.120709>. <insu-03629823>

HAL Id: insu-03629823

<https://insu.hal.science/insu-03629823v1>

Submitted on 4 Apr 2022

HAL is a multi-disciplinary open access archive for the deposit and dissemination of scientific research documents, whether they are published or not. The documents may come from teaching and research institutions in France or abroad, or from public or private research centers.

L'archive ouverte pluridisciplinaire HAL, est destinée au dépôt et à la diffusion de documents scientifiques de niveau recherche, publiés ou non, émanant des établissements d'enseignement et de recherche français ou étrangers, des laboratoires publics ou privés.



Distributed under a Creative Commons CC BY-NC-ND 4.0 - Attribution - Non-commercial use - No Derivative Works - International License

2
3 **The origin and dynamics of nitrogen in the Earth's mantle constrained by $^{15}\text{N}^{15}\text{N}$**
4 **in hydrothermal gases**

5 J. Labidi¹, E.D. Young²

6
7 ¹ Université de Paris, Institut de physique du globe de Paris, CNRS, Paris, France

8 ² Department of Earth, Planetary, and Space Sciences, UCLA, Los Angeles, CA, USA.
9

10 7,285 words, 7 figures

11
12 **Abstract**

13 The development of high-resolution gas source mass spectrometry has permitted
14 entirely new types of measurements of multiply-substituted isotopologues in gas species
15 of geochemical significance. Here, we present recent advances afforded by
16 measurements of $^{15}\text{N}^{15}\text{N}$ in natural samples, together with $^{14}\text{N}^{14}\text{N}$ and $^{15}\text{N}^{14}\text{N}$. We show
17 that the abundance of the doubly-substituted $^{15}\text{N}^{15}\text{N}$ isotopologue **in hydrothermal gases,**
18 **often mixtures of volatiles of widely different origins,** allows tracing the provenance of
19 nitrogen. The approach is based on the recent finding that atmospheric N_2 has a
20 substantial enrichment in $^{15}\text{N}^{15}\text{N}$ of nearly 20‰ relative to any other source of N_2 . This
21 is particularly useful for the study of hydrothermal gases, where characterizing the
22 isotopic composition and provenance of volcanic N_2 is important for a wide range of
23 applications in high-temperature geochemistry, but where air-derived N_2 is unavoidable.
24 In this review, we summarize the evidence that $^{15}\text{N}^{15}\text{N}$ is an unambiguous tracer of air

25 contamination. We compare two sets of published $^{15}\text{N}^{15}\text{N}$ data acquired on gases from
26 plume and arc volcanoes. We show how different sources of volcanic N_2 may be in plume
27 versus arc environments, and discuss the first-order constraints on the deep N cycle that
28 are provided by the new $^{15}\text{N}^{15}\text{N}$ data. Important findings include that the $\delta^{15}\text{N}$ tracer,
29 used alone or in conjunction with N_2/Ar and N_2/He ratios, can be surprisingly deceiving.
30 Isotope fractionation of atmospheric nitrogen occurs within hydrothermal systems,
31 resulting in negative $\delta^{15}\text{N}$ values similar to estimates for mantle values, yet with $^{15}\text{N}^{15}\text{N}$
32 values that preclude a mantle origin. The $^{15}\text{N}^{15}\text{N}$ data show that the true $\delta^{15}\text{N}$ of volcanic
33 components is positive in arcs but near-zero at the Yellowstone plume. In other words,
34 atmospheric N_2 can mimic mantle $\delta^{15}\text{N}$, and mantle $\delta^{15}\text{N}$ can look like the value of air.
35 Without $^{15}\text{N}^{15}\text{N}$, the apportioning of mantle and atmospheric N_2 in mixed gases can easily
36 be wrong. With $^{15}\text{N}^{15}\text{N}$, we also determine the true $\text{N}_2/{}^3\text{He}$ and $\text{N}_2/{}^{36}\text{Ar}$ ratios of volcanic
37 components in hydrothermal systems. Results inform our understanding of the deep
38 nitrogen cycle. Plume and arc volcanic endmembers show distinct isotope and elemental
39 ratios, consistent with sub-arc sources being overwhelmed by near-quantitative slab
40 **devolatilization**, while the Yellowstone plume source is not reflecting volatile subduction.

41

42 **1. Introduction**

43 Plate tectonics has shuffled the record of volatiles acquired by Earth's mantle during
44 planetary formation (Bekaert et al., 2021; Hilton et al., 2002; Jambon, 1994). Disambiguating
45 the relative importance of subducted and primordial volatiles in the global budget of the
46 deep Earth is crucial for a better understanding of planetary evolution. Information about
47 the N isotopic composition of Earth's mantle comes partly from basalts: quenching during

48 eruption of mid-ocean ridge basalts (MORB) on the seafloor results in the formation of glassy
49 rims preserving magmatic vesicles enriched in volatiles. These vesicles are a potential
50 treasure trove for sampling mantle volatiles. However, because nitrogen is a trace gas in
51 those vesicles, magmatic nitrogen contained within them is commonly contaminated by N₂-
52 rich air-derived components upon eruption (Marty, 1995; Marty and Zimmermann, 1999).
53 One strategy to see through the contamination by air has been to determine nitrogen isotope
54 ratios together with ⁴⁰Ar/³⁶Ar ratios (Marty, 1995). The rationale is that air and the mantle
55 have distinct ⁴⁰Ar/³⁶Ar ratios, ~ 300 and ~ 25,000 respectively (Moreira et al., 1998). Basalts
56 with ⁴⁰Ar/³⁶Ar ratios ~ 300 similar to air show evidence for air-derived nitrogen, while lavas
57 with ⁴⁰Ar/³⁶Ar ratios greater than ~1,000 appear to exhibit δ¹⁵N¹ values closer to true
58 mantle values (Marty, 1995; Marty and Zimmermann, 1999). Based on basalt studies, a δ¹⁵N
59 value of ~ -4‰ relative to air may be adopted as an estimate for the convective mantle (data
60 in Barry and Hilton, 2016; Cartigny et al., 2001; Javoy and Pineau, 1991; Marty, 1995; Marty
61 and Humbert, 1997; Marty and Zimmermann, 1999). Nitrogen in Earth's mantle is therefore
62 isotopically distinct from solar (δ¹⁵N ~ -400‰, Hashizume et al., 2000; Marty et al., 2011)
63 and from potential chondritic sources akin to enstatite chondrites (δ¹⁵N ~ -20‰ Grady et
64 al., 1986). The clear disagreement between mantle nitrogen and potential primordial
65 signatures has been suggested to reflect subduction of surface derived N with elevated δ¹⁵N
66 values, resulting in the departure from enstatite chondrites and/or solar δ¹⁵N values
67 towards higher δ¹⁵N over time (Barry and Hilton, 2016; Javoy, 1998; Marty and Dauphas,
68 2003; Williams and Mukhopadhyay, 2018). In other words, vestiges of primordial nitrogen

¹ δ¹⁵N refers to the per mil deviations in ¹⁵N/¹⁴N from the ratio in air.

69 acquired during Earth's accretion would have been erased with time by ongoing plate
70 tectonics. One requirement of this scenario is that surface nitrogen must have had $\delta^{15}\text{N} >$
71 20‰ in the Hadean and Archean, so that it can balance extremely low $\delta^{15}\text{N}$ for the primordial
72 mantle (Javoy, 1998). The consistently high $\delta^{15}\text{N}$ values in deep time are simply not observed
73 (Ader et al., 2016; Marty et al., 2013; Pinti et al., 2001), leaving the nitrogen deep cycle
74 unexplained.

75 Constraining the nitrogen isotopic compositions **of the sources of** mantle plumes and arc
76 volcanoes should help. Mantle plumes host primordial gases, undisturbed and isolated from
77 mantle convection for nearly 4.4 Gy, **mixed with subducted components** (Mukhopadhyay,
78 2012; Parai et al., 2019). Plume basaltic glasses are however **far less available than MORB,**
79 **and therefore less well understood.** Only seven plume basalts with $^3\text{He}/^4\text{He}$ ratios > 16 and
80 published $\delta^{15}\text{N}$ values pass the tests of having avoided **complete volatile overprinting by** air
81 contamination (i.e., non-air $^{40}\text{Ar}/^{36}\text{Ar}$ ratios). Those samples have $\delta^{15}\text{N}$ values between -2‰
82 and 0‰ (data in Marty and Dauphas, 2003; Marty and Humbert, 1997; Sano et al., 2001),
83 marginally higher than the convective mantle. Given the paucity of data, the influence of
84 subduction on the N budget of mantle plumes remains unclear. Nitrogen in arc mantle
85 sources is also important to study, as it is likely **influenced** by recycled surface-derived
86 components (Fischer et al., 2002; Füri et al., 2021; Taran, 2009). Sub-arc nitrogen may be
87 especially well suited for placing constraints on N isotope signatures that may be transferred
88 to the deep Earth. However, the N isotope compositions of sub-arc sources are even more
89 challenging to constrain because no glasses are available for analysis.

90 The study of volcanic gases offers a unique window into plumes and arc volatiles where
91 glasses are rare or absent. A large array of hot springs and fumaroles are vented to the

92 surface and reflect mixtures between surface waters, atmospheric gases, and variable
93 amounts of volcanic volatiles (Giggenbach, 1992). Instances of vented gases with plume-like
94 $^3\text{He}/^4\text{He}$ ratios are associated with $^{40}\text{Ar}/^{36}\text{Ar}$ ratios that remain under 1,000 (Boudoire et al.,
95 2020; Caliro et al., 2015; Chiodini et al., 2012; Sano et al., 1985). This is much lower than the
96 values of $\sim 5,000$ to $10,000$ thought to characterize the deep mantle (Mukhopadhyay, 2012;
97 Trieloff et al., 2000). Low $^{40}\text{Ar}/^{36}\text{Ar}$ in vented gases likely reflects a pattern of even greater
98 air contamination than evidenced in basalts. Gases emitted by arc volcanoes are also heavily
99 studied, but so far have shown $^{40}\text{Ar}/^{36}\text{Ar}$ ratios that are almost exclusively atmospheric
100 (Hilton et al., 2002; Pedroni et al., 1999; Sano and Fischer, 2013; Snyder et al., 2001). It is
101 unclear whether this reflects even more pronounced contamination directly from air, or
102 instead results from volcanic sources overwhelmed by subducted air-derived argon
103 (Staudacher and Allègre, 1988). In summary, gases from both plumes and arcs appear
104 dominated by atmospheric $^{40}\text{Ar}/^{36}\text{Ar}$ signatures, which is problematic for the identification
105 of volcanic N_2 in the gas mixtures.

106 As an alternative to relying on $^{40}\text{Ar}/^{36}\text{Ar}$ measurements alone as tracers of air
107 contamination, studies of fumaroles have often employed plots of $\delta^{15}\text{N}$ values versus bulk
108 N_2/Ar and N_2/He ratios, in part because these gas species ratios are easy to measure with
109 ordinary gas chromatography and quadrupole mass spectrometry techniques. In principle,
110 N_2/Ar and N_2/He ratios should allow the identification of mixing between mantle and
111 atmospheric endmembers, since air and various mantle sources are anticipated to be very
112 different (Elkins et al., 2006; Fischer et al., 2002, 1998; Roulleau et al., 2013; Sano et al., 2001,
113 1998; Taran, 2009; Zimmer et al., 2004). By design, the approach relies on the assumption
114 that $\delta^{15}\text{N}$, N_2/He and N_2/Ar ratios remain unfractionated, and are thus strictly tracers of

115 mixing in hydrothermal systems. Some of the most notable and vexing observations to date
116 using this method include: (1) various sub-arc regions show consistently positive $\delta^{15}\text{N}$ at
117 relatively high N_2/He and N_2/Ar ratios (Elkins et al., 2006; Fischer et al., 2002; Taran, 2011,
118 2009); (2) rare but remarkable occurrences of MORB $\delta^{15}\text{N}$ signatures in some arc volcanoes
119 (Fischer et al., 2002; Zimmer et al., 2004); (3) plume gases at Yellowstone with elevated
120 $^3\text{He}/^4\text{He}$ ratios and $\delta^{15}\text{N}$ values clustered around 0‰, the value of air, even at N_2/He ratios
121 five orders of magnitude below the value of the atmosphere (Chiodini et al., 2012); and (4)
122 other plume gases, from both Iceland and Azores, also with elevated $^3\text{He}/^4\text{He}$ but higher
123 N_2/He (i.e., closer to air) and negative $\delta^{15}\text{N}$ values as low as -10‰ , nominally inconsistent
124 with the signature of contaminant air (Caliro et al., 2015; Marty et al., 1991; Sano et al., 1985).
125 In the latter case, the surprisingly low $\delta^{15}\text{N}$ values were interpreted as either reflecting a
126 unique feature of the high $^3\text{He}/^4\text{He}$ mantle, resembling of the values for enstatite chondrites
127 (Caliro et al., 2015; Marty et al., 1991) or as the result of N isotopic fractionation of
128 atmospheric N_2 in the hydrothermal systems (Marty et al., 1991). Overall, it is hard to
129 reconcile $\delta^{15}\text{N}$ values with high $^3\text{He}/^4\text{He}$ from one site to another. What is clear from this
130 brief literature review is that the nitrogen isotope geochemistry of hydrothermal fluids is
131 potentially of great utility for constraining the cycle of nitrogen in the deep Earth, but simple
132 conclusions are hindered by pervasive air contamination.

133 The burgeoning field commonly referred to as “clumped” isotope geochemistry makes
134 use of the relative abundance of multiply-substituted isotopologues in a given molecule, i.e.,
135 the abundance of isotopic molecular species with more than one heavy isotope substitution
136 (hence the term “clumping” of isotopes). A number of molecules have been investigated,
137 although studies of rare isotopologues of CO_2 and CH_4 dominate the field. The main goal in

138 many of these studies has been to derive temperatures of formation of carbonate minerals
139 (in the case of CO₂ liberated from carbonates) or the origins of various gases, with an
140 emphasis on the potential biogenicity of the gases in the case of CH₄ (Henkes et al., 2018;
141 Young et al., 2017). Here we describe a somewhat different application in which isotope
142 clumping is a unique tracer of provenance, in this case ¹⁵N¹⁵N in N₂ gas in volcanic systems.
143 This tracer arises because of an extraordinary disequilibrium overabundance of ¹⁵N¹⁵N in
144 air. In this review, we summarize work to date that illustrates how the ¹⁵N¹⁵N novel tracer
145 places new constraints on air contamination of hydrothermal samples (Labidi et al., 2021,
146 2020; Yeung et al., 2017). We present observations and constraints from our recent studies
147 of the rare isotopologue ¹⁵N¹⁵N in nitrogen from hydrothermal gases worldwide,
148 representing both plumes and arcs. Recently published ¹⁵N¹⁵N data offer a distinctive
149 perspective on nitrogen recycling in these various geodynamic settings. We summarize the
150 evidence that the new ¹⁵N¹⁵N tracer is an unambiguous indicator of air contamination for
151 nitrogen, much more so than δ¹⁵N alone, ⁴⁰Ar/³⁶Ar ratios, or even δ¹⁵N associated with N₂/He
152 and N₂/Ar ratios. In this review, we discuss new evidence that δ¹⁵N and N₂/Ar fractionations
153 are at play in hydrothermal systems. We identify the composition of volcanic N₂ in the plume
154 and arc environments, and discuss the first-order constraints on the deep N cycle that are
155 provided by the new ¹⁵N¹⁵N data.

156

157 2. ¹⁵N¹⁵N: an air tracer *par excellence*

158 The doubly-substituted isotopologue ¹⁵N¹⁵N is an example of a “clumped” isotopic
159 species, a term often invoked in the geochemical literature to describe isotopic molecular
160 species (isotopologues) with more than one heavy isotope. The application of ¹⁵N¹⁵N to

161 tracing the provenance of volcanic gases is based on the recent discovery that atmospheric
 162 nitrogen possesses a considerable $^{15}\text{N}^{15}\text{N}$ enrichment of nearly 2% (Yeung et al., 2017),
 163 making air easy to distinguish from any magmatic nitrogen or nitrogen produced by other
 164 geochemical or biological processes. In the laboratory, we measure $^{29}\text{N}_2/^{28}\text{N}_2$ and $^{30}\text{N}_2/^{28}\text{N}_2$
 165 ratios and report them as $\delta^{29}\text{N}_2$ and $\delta^{30}\text{N}_2$, the per mil deviations from air. In the case of
 166 $^{29}\text{N}_2/^{28}\text{N}_2$ $\delta^{29}\text{N}_2 = 1000 \times ((^{29}\text{R}_{\text{sample}}/^{29}\text{R}_{\text{air}} - 1) (\text{‰}))$ where $^{29}\text{R} = (^{14}\text{N}^{15}\text{N} + ^{15}\text{N}^{14}\text{N})/^{14}\text{N}^{14}\text{N}$ for
 167 the gas of interest. Since $(^{14}\text{N}^{15}\text{N} + ^{15}\text{N}^{14}\text{N})/^{14}\text{N}^{14}\text{N}$ equals $2(^{15}\text{N}/^{14}\text{N})$ for both the sample and
 168 the standard, for all practical purposes, $\delta^{29}\text{N}_2$ is equivalent to the bulk isotope ratio
 169 expressed as $\delta^{15}\text{N} = 1000 \times (^{15}\text{R}_{\text{sample}}/^{15}\text{R}_{\text{air}} - 1)$. For $^{30}\text{N}_2/^{28}\text{N}_2$, $\delta^{30}\text{N}_2 =$
 170 $1000 \times (^{30}\text{R}_{\text{sample}}/^{30}\text{R}_{\text{air}} - 1) (\text{‰})$ where $^{30}\text{R} = ^{15}\text{N}^{15}\text{N}/^{14}\text{N}^{14}\text{N}$ for a given sample. In general,
 171 simple fractionation by molecular weight of N_2 will result in variations in $\delta^{30}\text{N}_2$ that are
 172 roughly twice the variations in $\delta^{29}\text{N}_2$ (see below).

173 The Δ_{30} tracer is a measure of departures from a purely stochastic distribution of ^{15}N and
 174 ^{14}N atoms comprising the isotopic molecular species. It is defined such that $\Delta_{30} =$
 175 $1000 \times (^{30}\text{R}/(^{15}\text{R})^2 - 1) (\text{‰})$, where $^{15}\text{R} = ^{15}\text{N}/^{14}\text{N}$ for the gas of interest. The value $(^{15}\text{R})^2$
 176 represents the stochastic relative abundance of $^{30}\text{N}_2$, and reflects the fact that the probability
 177 of forming $^{30}\text{N}_2$ from a purely random distribution of ^{14}N and ^{15}N atoms across all nitrogen
 178 isotopologues is the square of the probability of finding molecules with just one ^{15}N
 179 (concentrations are in effect probabilities in the stochastic limit). Of course, the formation of
 180 $^{15}\text{N}^{15}\text{N}$ is not necessarily purely random. The low vibrational energy of this doubly-
 181 substituted molecule results in a thermodynamic driving force for its formation. The
 182 thermodynamic favorability for $^{15}\text{N}^{15}\text{N}$ formation is strongest at the lower temperatures. At
 183 geochemically relevant temperatures ranging from 200 to 1000 °C, equilibrium among N_2

184 isotopologues results in Δ_{30} values from 0.5 to 0.1‰, respectively (Yeung et al., 2017). This
185 applies for any N_2 molecule made in a geological process, whether it is mantle-derived or
186 inherited from slabs, for example (Labidi et al., 2020).

187 In contrast to expectations from equilibrium thermodynamics and normal, purely mass-
188 dependent fractionation processes, air has a pronounced disequilibrium enrichment in
189 $^{15}N^{15}N$, leading to an atmospheric Δ_{30} value of $19.1 \pm 0.3\text{‰}$ (2σ) (Yeung et al., 2017). The Δ_{30}
190 value of air behaves as an indelible signature that is an isotopologue (molecular) analogue
191 of the three-isotope anomaly that has proven so useful in oxygen isotopes, $\Delta^{17}O$ (e.g., Clayton
192 and Mayeda, 1984): it is not erased by mass-dependent fractionation of N_2 and is not re-
193 ordered in heated hydrothermal systems (see appendix C). The use of Δ_{30} as a tracer of air
194 does not require any assumptions about the relative abundances of other tracers, as is the
195 case for $^{40}Ar/^{36}Ar$ or N_2/Ar ratios. Instead, we use the isotopic compositions of the N_2
196 molecules themselves to trace the origin of the nitrogen in a manner that is more diagnostic
197 than $\delta^{15}N$. Based on the application of this tracer to volcanic hydrothermal systems, we show
198 that both $\delta^{15}N$ and N_2/Ar experience fractionations in natural hydrothermal systems, and
199 that atmospheric-like $^{40}Ar/^{36}Ar$ ratios may be genuine features of the sub-arc mantle.
200 Ultimately, previously unrecognized fractionation of $^{15}N/^{14}N$ (expressed as shifts in $\delta^{15}N$)
201 and N_2/Ar appear to have conspired to produce deceptive indicators for the origin of N in
202 gas mixtures that Δ_{30} measurements can help rectify.

203 In what follows we illustrate the potency of $^{15}N^{15}N$ to constrain the true $\delta^{15}N$, $N_2/^{36}Ar$,
204 $N_2/^{3}He$, $^{40}Ar/^{36}Ar$, and even $^3He/^{36}Ar$ ratios of volcanic components contributing to
205 hydrothermal gases. The new $^{15}N^{15}N$ data offer valuable constraints on the deep-Earth cycles

206 of both nitrogen and argon, especially when associated with conventional noble gases
207 measurements.

208

209 **3. Measurements of isotope ratios at high mass resolution: the challenge of**

210 **$^{15}\text{N}^{15}\text{N}$**

211 Measurements of nitrogen isotopologues involve high-mass-resolution mass
212 spectrometry. The abundances of $^{14}\text{N}^{14}\text{N}^+$, $^{14}\text{N}^{15}\text{N}^+$ (representing both isotopomers, $^{14}\text{N}^{15}\text{N}$
213 and $^{15}\text{N}^{14}\text{N}$) and $^{15}\text{N}^{15}\text{N}^+$ ions are measured with high mass resolution to avoid mass-to-
214 charge interferences. Interferences for $^{28}\text{N}_2$ ($^{14}\text{N}^{14}\text{N}^+$) and $^{29}\text{N}_2$ ($^{14}\text{N}^{15}\text{N}^+$) are from carbon
215 monoxide, ^{28}CO ($^{12}\text{C}^{16}\text{O}^+$) and ^{29}CO ($^{13}\text{C}^{16}\text{O}^+$ and $^{12}\text{C}^{17}\text{O}^+$). The $m/\Delta m$ separating ^{28}CO
216 ($^{12}\text{C}^{16}\text{O}^+$) from $^{28}\text{N}_2$ ($^{14}\text{N}^{14}\text{N}^+$) is $\sim 2,500$, while values of $\sim 6,000$ and $\sim 7,000$ separate $^{13}\text{C}^{16}\text{O}^+$
217 and $^{12}\text{C}^{17}\text{O}^+$ from $^{29}\text{N}_2^+$, respectively. Based on the zero-order rule that mass resolving power
218 (instrumental $m/\Delta m$) must be $\sim 3 \times m/\Delta m$ between the species, mass resolving powers of at
219 least 7,500, 18,000 and 21,000, respectively, are required to separate N_2 from interferences
220 on nominal masses 28 and 29. In the case of mass/charge 30, low backgrounds of nitrogen
221 monoxide (NO^+) are ubiquitous and require a sufficiently high mass resolution to separate
222 $^{30}\text{NO}^+$ from $^{30}\text{N}_2^+$. The $m/\Delta m$ between $^{30}\text{NO}^+$ and $^{30}\text{N}_2^+$ is $\sim 13,400$, requiring an instrumental
223 **mass resolving power** of at least $\sim 45,000$.

224 At the time of this writing, and to the best of our knowledge, $^{30}\text{N}_2$ measurements have
225 been performed only at the University of California, Los Angeles (UCLA) on a *Nu Instruments*
226 Panorama. Routine measurements at mass resolving powers above 50,000 are achieved with
227 an entrance slit width of about 30 μm . A mass spectrum of the $^{30}\text{N}_2^+$ beam under working
228 conditions is shown in Young et al. (2016). $^{30}\text{N}_2^+$ ions are detected using a secondary electron

229 multiplier, with count rates of between 5,000 and 40,000 cps for most natural samples. Ions
230 with m/z of 28 and 29 are measured using Faraday cups with $10^{11} \Omega$ amplifier resistors.

231 Natural samples from the field show a broad range of N_2 concentrations, typically from
232 0.01 vol% N_2 to 80 vol% N_2 . These concentrations translate into between 1 and 500 μ moles
233 of N_2 for published Δ_{30} analyses. Counting times are adjusted to account for the large range
234 in sample N_2 concentrations. This results in variable analytical precision from one sample to
235 another. Samples yielding $\geq 5 \mu$ moles of N_2 permit conventional dual-inlet measurements,
236 with analysis times of up to 7.5 hours to yield the best precision. For samples with $< 5 \mu$ moles
237 of N_2 , measurements have been performed by concentrating on a liquid-nitrogen
238 “microvolume”, with analysis times of 1 hour at most. For analyses lasting 7.5 hours, internal
239 precision for Δ_{30} values is typically $\leq 0.2\text{‰}$ (1 s.e.). Samples with less than 5 μ moles N_2 yield
240 internal uncertainties of between 0.18 and 1.80 ‰ (1 s.e.).

241

242 4. $^{15}N^{15}N$ composition of N_2 in nature

243 The published data for natural samples for which we have obtained Δ_{30} values are from
244 Yeung et al., (2017), Labidi et al. (2020) and Labidi et al. (2021). They are shown in a plot of
245 $\delta^{29}N_2$ versus $\delta^{30}N_2$ in Fig. 1 and as Δ_{30} versus $\delta^{15}N$ in Fig. 2. Published data summarized here
246 include samples of air N_2 , as well as magmatic, hydrothermal and crustal gases (see Yeung et
247 al. 2017 for analyses of biologically-produced N_2 which have Δ_{30} values within $\sim 1 \text{‰}$ of
248 zero). The dataset is dominated by hydrothermal samples (n=48) but also features
249 measurements of magmatic (n=4, MORB in figure 1) and crustal fluids (n=5, mine gases in
250 figure 1). Magmatic samples were extracted from mid-ocean ridge basalts with high volatile
251 content (n=4). Crustal gases are extracted from fractures at depth, from the Canadian shield

252 (n=5). Hydrothermal samples are from plumes and arcs from Halemaumau (n=1, Hawaii),
253 various locations within Iceland (n=11), the Yellowstone caldera (n=13, USA), the Eifel
254 region (n=5, Germany), and the Momotombo (n=2, Nicaragua), Santa Ana (n=1, El Salvador),
255 and Poás (n=5, Costa Rica) volcanos **as well from an array of springs** from Costa Rica and
256 Panama **(n=6)**.

257 The data reveal patterns dominated by the presence or absence of the atmospheric Δ_{30}
258 signature. In Fig. 1, correlated variations of $\delta^{30}\text{N}_2$ against $\delta^{29}\text{N}_2$ are observed on two parallel
259 lines with slopes of ~ 2 , as expected where fractionation by molecular mass occurs. The
260 upper line corresponds to air and samples fractionated from air, and the lower line includes
261 samples unrelated to air that have equilibrium (or near equilibrium) concentrations of
262 $^{15}\text{N}^{15}\text{N}$. The slope of ~ 2 results from the mass differences between $^{30}\text{N}_2$, $^{29}\text{N}_2$, and $^{28}\text{N}_2$. For
263 example, diffusion of these molecules would lead to fractionation factors $\alpha_{29/28}$ and $\alpha_{30/28}$
264 (e.g., $\alpha_{29/28} = (^{29}\text{N}_2/^{28}\text{N}_2)_{\text{diffused}} / (^{29}\text{N}_2/^{28}\text{N}_2)_o$) for $^{29}\text{N}_2/^{28}\text{N}_2$ and $^{30}\text{N}_2/^{28}\text{N}_2$ of $\sqrt{(m^{28}\text{N}_2/m^{29}\text{N}_2)}$
265 and $\sqrt{(m^{28}\text{N}_2/m^{30}\text{N}_2)}$, respectively (Graham's law), where $m^{28}\text{N}_2$ is the molecular mass of
266 $^{28}\text{N}_2$, and so forth. In general, $\alpha_{29/28} = \alpha_{30/28}^\beta$ where in this case $\beta = \ln(m^{28}\text{N}_2/m^{30}\text{N}_2) /$
267 $\ln(m^{28}\text{N}_2/m^{39}\text{N}_2) = 0.5085$ (Young et al., 2002). Because shifts in delta values are related to
268 fractionation factors by $\delta - \delta_o \sim 10^3 \ln(\alpha)$, the slope relating variations in $\delta^{30}\text{N}_2$ to $\delta^{29}\text{N}_2$ in Fig.
269 1 is $\sim 1/\beta$ or 1.966. Various examples of mixtures plot between the two lines.

270 The two lines are separated by the $\sim 19\text{‰}$ offset for air (Fig. 1). Gases heated in the
271 laboratory between 400 and 1,000 °C reflect equilibrium bond-ordering with values of Δ_{30}
272 near zero. We take the gases at 1,000 °C that plot on the lower line as useful representatives
273 of the stochastic distribution of N_2 isotopologues. Figure 1 underscores the striking nature
274 of the anomalous $^{30}\text{N}_2$ in air; temperatures ranging from 25 to 1000 °C should result in

275 Δ_{30} values from 1.1 to 0.1‰, respectively (Yeung et al., 2017). The ~19‰ disequilibrium
276 $^{15}\text{N}^{15}\text{N}$ excess for atmospheric N_2 is likely due to nitrogen photochemistry in the modern
277 upper atmosphere (Yeung et al., 2017). The mechanism responsible for the enrichment
278 evidently requires the presence of O_2 during N_2 photolysis, so predictions could be made for
279 planetary atmospheres containing N_2 but no O_2 , including Earth's atmosphere prior to the
280 great oxygenation event. Most importantly for this review, the $^{15}\text{N}^{15}\text{N}$ enrichment in air is an
281 unambiguous measure of air in mixed gases.

282 Analysis of a variety of natural samples of nitrogen show mass fractionation of
283 molecular species is rife, as evidenced by slope-2 variability in $\delta^{30}\text{N}_2$ vs. $\delta^{29}\text{N}_2$ space (Fig. 1).
284 Importantly for this work on volcanic hydrothermal systems, the array of mass-dependent
285 signatures going through air indicates air-derived N_2 experiences mass fractionation in
286 nature. This is an important observation; nitrogen derived from air does not have a single
287 $\delta^{29}\text{N}$ (or $\delta^{15}\text{N}$) because N_2 can be fractionated by molecular mass. The mass fractionation
288 array defined by gases with equilibrium, or nearly equilibrium, Δ_{30} values result from
289 fractionation during geological and/or biological processing (Fig. 1).

290 In figure 2, Δ_{30} values are plotted against $\delta^{29}\text{N}_2$. Because $\delta^{29}\text{N}_2$ is numerically equal to
291 $\delta^{15}\text{N}$, all plots going forward directly use the $\delta^{15}\text{N}$ notation instead of $\delta^{29}\text{N}_2$. N_2 may be
292 produced during volcanic degassing, but also during metamorphism or thermogenic
293 cracking. Δ_{30} values of ~ 0‰ are expected for N_2 molecules from magmas because at high
294 temperatures, thermodynamic equilibrium approaches the random distribution of $^{15}\text{N}^{15}\text{N}$
295 relative to other N_2 isotopologues. This was verified by the study of mid-ocean ridge basalts
296 with extraordinarily high volatile concentrations. Crushing experiments under vacuum
297 released N_2 with Δ_{30} values between $+1.2 \pm 2.6\text{‰}$ and $+3.0 \pm 3.6\text{‰}$ (Fig. 2, Labidi et al., 2020).

298 These data confirm that magmatic N₂ formed by degassing at ~ 1200 °C has Δ₃₀ ~ 0‰. The
299 mechanism for N₂ formation in crustal environments is breakdown of NH₄-bearing
300 phyllosilicates at peak metamorphic temperatures (Li et al., 2021). Gases from two deep
301 mines in the Canadian shield have Δ₃₀ values between 1.1±0.4‰ and 0.5±0.2‰ (2 σ, n=2).
302 These data confirm that crustal generation of N₂ by metamorphism has Δ₃₀ values < 1‰ as
303 expected for approaches to thermodynamic equilibrium.

304

305 5. The Δ₃₀ – δ¹⁵N evidence that air is ubiquitous and fractionated

306 By way of summary, we can say that high-temperature N₂ is characterized by Δ₃₀ of
307 ~0‰ and variable δ¹⁵N, and that air-derived N₂ has a Δ₃₀ value of 19‰ and can also have
308 variable δ¹⁵N (Fig. 2). A number of samples exhibit Δ₃₀ values intermediate between air and
309 stochastic. Because there is no primary mechanism for producing intermediate values, these
310 samples must be mixtures between air and high-temperature, volcanic N₂ (see appendix C
311 for evidence against Δ₃₀ re-ordering in nature). In principle, mixing between two N₂ gases
312 with very different δ¹⁵N values but similar, near-equilibrium Δ₃₀ values can produce
313 anomalously high Δ₃₀ values (i.e., mixing relationships are curves, not straight lines). In
314 practice however, the differences in δ¹⁵N values required to produce mixing curves with
315 sufficient curvature to cause discernible aberrations in Δ₃₀ are on the order of hundreds of
316 permil (Yeung et al., 2017 – also, see appendix).

317 Because mixing in Δ₃₀ – δ¹⁵N space is effectively linear, it is straightforward to identify
318 endmember N₂ compositions for mixtures. For hydrothermal samples with Δ₃₀ values of
319 19‰, virtually all N₂ in the gas mixture is derived from air. Atmospheric Δ₃₀ values dominate

320 most (but not all) hot spring data. This likely reflects the recharge of surficial hydrothermal
321 systems by air-saturated meteoric fluids, causing atmospheric N₂ to dominate over high-
322 temperature N₂. Gases from Iceland, the Yellowstone caldera, and the Poás volcano all show
323 atmospheric Δ₃₀ values but negative δ¹⁵N down to -10‰ (Fig. 3). The negative δ¹⁵N values
324 are deceptively similar to the MORB value of -4±2‰ (Javoy and Pineau, 1991, Marty et al.,
325 1999), but the Δ₃₀ values preclude a magmatic origin. The negative δ¹⁵N signatures must
326 result from isotopic fractionation of air. The distribution of δ²⁹N₂ and δ³⁰N₂ along a slope of
327 ~2 in Fig. 1 indicates mass fractionation of the air-derived nitrogen. The fractionation likely
328 occurs in the sub-surface, after air-saturated meteoric waters feed atmospheric nitrogen into
329 hydrothermal systems. Upon heating, fluids undergo water/gas partitioning, eventually
330 resulting in volatile losses. If water/gas exchange is associated with a ¹⁵N/¹⁴N fractionation,
331 the degassed fluids would have ¹⁵N/¹⁴N ratios (δ¹⁵N values) distinct from that of the residual
332 N₂ left in the geothermal waters. Air with δ¹⁵N values between -5 and -10‰ indicate two
333 alternative possibilities:

- 334 (1) N isotope fractionation factors are similar to Graham's law, resulting in the
335 instantaneous release of N₂ greatly depleted in ¹⁵N, while residual N₂ is enriched in
336 ¹⁵N, depending on the extent of degassing; or
- 337 (2) N isotope fractionations are smaller than suggested by Graham's law, but amplified
338 by open-system Rayleigh distillations, in which both the product and the residue of
339 the water/gas fractionation are drawn to low δ¹⁵N as the proportion of N held by
340 the aqueous phase decreases.

341 In case 1, where fractionation occurs as a single-step process, the fractionation factor
342 for isotopologue partitioning could be as great as the inverse of the square root of the inverse

343 of the isotopologue mass ratio, which would result in $\delta^{29}\text{N}_2$ (or $\delta^{15}\text{N}$) for the effusing gas that
344 is -17‰ lower than that of the aqueous phase. The residual nitrogen in the fluid would have
345 a complimentary enriched $\delta^{29}\text{N}_2$ (or $\delta^{15}\text{N}$) value. By simply propagating a 17‰ fractionation
346 between dissolved and exsolved N_2 , one expects the low $\delta^{15}\text{N}$ of -6‰ seen in the Iceland
347 dataset from Labidi et al., (2020) to eventually produce the complimentary high $\delta^{15}\text{N}$ values
348 of $+11\text{‰}$, but these are not seen. The most positive $\delta^{15}\text{N}$ at an atmospheric Δ_{30} is only
349 $+0.5\text{‰}$ in Icelandic fumaroles (Fig. 3). A single-step process therefore seems unlikely, and
350 this is supported by experiments. The $^{15}\text{N}/^{14}\text{N}$ isotope fractionation between N_2 gas and N_2
351 dissolved in aqueous fluid, $\alpha = (^{29}\text{R})_{\text{gas}}/(^{29}\text{R})_{\text{fluid}}$, when expressed as $\delta^{15}\text{N}_{\text{gas}} - \delta^{15}\text{N}_{\text{fluid}}$, is found
352 to range from -0.9 to $+0.4\text{‰}$ from 6 to 60 °C (Lee et al., 2015). The reversal of the
353 fractionations at 40 °C indicates the N_2 isotope fractionation factors result from a kinetic
354 rather than an equilibrium process, and that the kinetic fractionation is fundamentally
355 different from the simple square-root of the inverse mass ratio. Above 40 °C , isotopically
356 light N_2 is preferentially partitioned into the aqueous fluid phase, and isotopically heavy N_2
357 resides in the gaseous phase (Lee et al., 2015). Linear extrapolation to 100 °C results in a
358 fractionation of $+1.0\text{‰}$. With this fractionation, Rayleigh distillation would push the product
359 and the residue to $\delta^{15}\text{N}$ values as low as -5‰ and -6‰ , for gas and fluid, with $\sim 99\%$ N_2
360 degassing. The possibility of a higher fractionation would change the exact fractions of
361 degassed nitrogen, but would not fundamentally modify our main hypothesis: N_2 isotope
362 fractionations in hydrothermal systems are to be expected as the result of significant
363 degassing in the absence of meteoric, air-saturated water recharge.

364 There is also evidence that the fractionations of $\delta^{15}\text{N}$ in air-derived N_2 are variable on
365 human timescales. In Iceland, fractionated air was observed with $\delta^{15}\text{N}$ values as low as -6‰

366 for gases sampled in 2018 (Labidi et al., 2020). Fumaroles sampled elsewhere in Iceland in
367 1982 (Sano et al., 1985) had $\delta^{15}\text{N}$ values down to -10‰ (Marty et al., 1991). At Poás,
368 fumaroles sampled between 1998 and 2001 produced unfractionated air with $\delta^{15}\text{N} = 0\text{‰}$
369 (Vaselli et al., 2003), while field expeditions a few months later in 2001, and in 2006–2007,
370 the same fumaroles yielded negative $\delta^{15}\text{N}$ values of -3‰ (Fischer et al., 2015, 2002;
371 Zimmer et al., 2004). The latter samples tend to have atmospheric Δ_{30} values (Labidi et al.,
372 2021), demonstrating the negative $\delta^{15}\text{N}$ are due to fractionation of atmospheric N_2 .
373 Similarly, at Yellowstone, a field expedition in September 2007 (Chiodini et al., 2012) yielded
374 no measurable $\delta^{15}\text{N}$ fractionation. Samples taken in August 2018 in the same hydrothermal
375 vents resulted in greatly fractionated air signatures with $\delta^{15}\text{N}$ as low as $\sim -10\text{‰}$ (Labidi et
376 al., 2020). The $\delta^{15}\text{N}$ variability of air-derived N_2 should be a subject of future dedicated
377 studies. The time variability of $\delta^{15}\text{N}$ in N_2 derived from air in hydrothermal systems is
378 particularly problematical for using $\delta^{15}\text{N}$ as a tracer for the provenance of N_2 . In the interim,
379 very negative $\delta^{15}\text{N}$ in hydrothermal systems should be regarded as a natural consequence of
380 degassing in the context of intermittent meteoric (air-saturated) water recharge. In all cases,
381 $\delta^{15}\text{N}$ alone in hydrothermal gases is a poor tracer of the origin of N_2 . In the absence of $^{15}\text{N}^{15}\text{N}$
382 data, $\delta^{15}\text{N}$ alone may lead to erroneous conclusions regarding the origin of volatiles in
383 hydrothermal gases.

384

385 6. Identifying high-temperature N_2

386 Gases from Yellowstone, Eifel, and Central America all incorporate some high-
387 temperature N_2 with $\Delta_{30} \sim 0$, resulting in variable Δ_{30} values due to mixing with air.

388 Extrapolation of trends in data to $\Delta_{30} = 0$ ‰ constrains the volcanic endmembers for $\delta^{15}\text{N}$
389 (Fig. 3), $\text{N}_2/{}^3\text{He}$ (Fig. 4), $\text{N}_2/{}^{36}\text{Ar}$ (Fig. 5) and ${}^{40}\text{Ar}/{}^{36}\text{Ar}$ (Fig. 6). Some of the main conclusions
390 on high-temperature volatiles are summarized in a cartoon on Fig. 7.

391 Eifel gases happen to be the simplest to interpret of the entire Δ_{30} dataset because they
392 have Δ_{30} values as low as 0.3 ± 0.7 ‰, i.e., within uncertainty of 0 ‰, requiring no
393 extrapolation whatsoever to determine the $\delta^{15}\text{N}$ of high-temperature N_2 . For those gases, the
394 high-temperature $\delta^{15}\text{N}$ value is -1.2 ± 0.5 ‰, a value that is slightly higher than estimates for
395 the average for MORB mantle of $\sim -4 \pm 2$ ‰ (Javoy and Pineau, 1991; Marty and
396 Zimmermann, 1999). This marginally higher value could indicate the addition of recycled
397 nitrogen with positive $\delta^{15}\text{N}$ in the Eifel mantle source (Labidi et al., 2020).

398 At Poás and Momotombo, two volcanoes from Central America, Δ_{30} values range down
399 to $+3.4 \pm 1.0$ and 1.5 ± 0.3 ‰. Extrapolation of the linear fits to Δ_{30} values of zero suggests that
400 the volcanic N_2 at Poás and Momotombo have $\delta^{15}\text{N}$ values of $\sim +1 \pm 0.5$ ‰ and $\sim +5 \pm 0.5$ ‰
401 respectively (Labidi et al., 2021). It is unclear whether the Poás endmember reflects a unique
402 volcanic endmember across central America, or a fractionated value, disconnected from the
403 magmatic signature (Labidi et al., 2021). Overall, in view of the expectation that slab-derived
404 nitrogen should have $\delta^{15}\text{N}$ values of near $+5$ ‰ (Busigny et al., 2011; Li and Bebout, 2005),
405 these high-T estimates are consistent with the addition of recycled N in the central American
406 sub-arc mantle.

407 For Yellowstone, the Δ_{30} values range down to 3.8 ± 1.7 ‰, but the $\delta^{15}\text{N}-\Delta_{30}$ scatter is
408 substantial (Fig. 3). An extrapolation of the $\delta^{15}\text{N}-\Delta_{30}$ data to $\Delta_{30} = 0$ was carried out by Labidi
409 et al., (2020) using only the data comprising the steep negative sloping array, resulting in an

410 estimate for volcanic $\delta^{15}\text{N}$ of $+3\pm 2\text{‰}$ (Labidi et al., 2020). Given the magnitude of the $\delta^{15}\text{N}$ -
411 Δ_{30} scatter, it is unclear whether this extrapolation is valid. The alternative, more
412 conservative approach is to use the sample with the lowest Δ_{30} to define a minimum $\delta^{15}\text{N}$
413 of $\sim +0.2\text{‰}$. Higher values suggested by Labidi et al., (2020) are possible, but are not required
414 by the data as a whole on Fig. 3. We note that a high-temperature endmember with $\delta^{15}\text{N}\sim$
415 0‰ is consistent with the data from Chiodini et al., (2012) for Yellowstone, perhaps lending
416 support for the more conservative approach.

417 Overall, based on our Δ_{30} values from the fumaroles sampled thus far, we find high
418 $\delta^{15}\text{N}$ in high-temperature components compared to MORB nitrogen (Fig. 7). Elevated
419 $^{15}\text{N}/^{14}\text{N}$ isotope signatures may reflect the addition of nitrogen recycled from the downgoing
420 slab, as suggested in the literature (Barry and Hilton, 2016; Bebout and Fogel, 1992; Busigny
421 et al., 2003; Dauphas and Marty, 1999). To constrain whether subducted nitrogen is added
422 to the sources of plumes and/or arc source, we make use of $\text{N}_2/^{36}\text{Ar}$ and $\text{N}_2/^{3}\text{He}$ ratios.

423

424

425 **7. Coupling $^{15}\text{N}^{15}\text{N}$ and ^{36}Ar data: important but challenging**

426 The ratios N_2/Ar and $\text{N}_2/^{36}\text{Ar}$ are used routinely as tracers of volatile origin, and are
427 also important data for calculating fluxes of N_2 outgassing. Published $\text{N}_2/^{36}\text{Ar}$ data with Δ_{30}
428 values are shown on Fig. 5 and the significance of the potential correlations are discussed in
429 the following section. We also present combinations of Δ_{30} data with $^{40}\text{Ar}/^{36}\text{Ar}$ (Fig. 6) and
430 discuss the intricacies of the ^{36}Ar - N_2 geochemical pair, as revealed by $^{15}\text{N}^{15}\text{N}$ data.

431

432 7.1 Using $^{15}\text{N}^{15}\text{N}$ to determine $\text{N}_2/^{36}\text{Ar}$ ratios

433 The first important observation on Fig. 5 is that at atmospheric Δ_{30} , $N_2/^{36}Ar$ ratios are
434 variable. They range from the nominal value for air of $\sim 2.5 \times 10^4$ to $\sim 0.4 \times 10^4$. The low end of
435 the range is three times below the anticipated $N_2/^{36}Ar$ for air-saturated waters of $\sim 1.2 \times 10^4$.
436 This is likely the result of hydrothermal degassing described in section 6. The solubilities of
437 argon and nitrogen are distinct by about a factor of 2 in geothermal waters, at temperatures
438 between 20 and 100 °C (Ballentine et al., 2002). Assuming hydrothermal degassing occurs
439 as a Rayleigh distillation process, and using the solubility relationships reviewed in
440 Ballentine et al., (2002), 95% N_2 degassing would be associated with 75% Ar degassing,
441 causing $N_2/^{36}Ar$ of the residual fluids to be fractionated (lowered) by a factor of ~ 3 relative
442 to the starting composition (Labidi et al., 2021). The discovery that degassing fractionates
443 N_2/Ar ratios is important with respect to the use of nitrogen excesses, N_2^* , introduced by
444 Fischer et al., (1998). Excess nitrogen is defined as $[N_2^*] = [N_2]_{\text{measured}} - 40 \times [Ar]_{\text{measured}}$. The
445 numerical value 40 corresponds to the N_2/Ar ratio of air-saturated water. It is an important
446 notion, used to pro-rate the bulk flux of N_2 to obtain the volcanic fraction only, in entire arcs
447 (Fischer et al., 2002). Any $N_2/Ar > 40$ is thought to reflect the contribution of volcanic
448 nitrogen with high N_2/Ar added to unfractionated air-saturated waters. The prospect that
449 atmospheric components in fact have variable N_2/Ar likely warrants revisiting the notion of
450 N_2^* .

451 The relationships between $N_2/^{36}Ar$ and Δ_{30} can be projected to high-temperature
452 endmembers with $\Delta_{30} = 0\text{‰}$, to estimate the $N_2/^{36}Ar$ ratio of the volcanic gases. Yellowstone
453 fumaroles characterized by air-like $N_2/^{36}Ar$ span nearly the entire range of Δ_{30} values (Fig.
454 5A). However, having taken into account the variable degrees of elemental fractionation of
455 air prior to mixing, the Yellowstone dataset is reasonably consistent with a high $N_2/^{36}Ar$ of

456 $\sim 10^6$, similar to MORB (Fig. 5A). Fumaroles from the Central America subduction zone are
457 far more ambiguous. The data distribution can be fit with a high-temperature endmember
458 with $N_2/^{36}\text{Ar}$ anywhere between $\sim 10^6$ (similar to MORB, Fig. 5A) and $\sim 10^4$ (similar to air,
459 fig. 5B). These ratios have vastly different implications for the volatile budget and fluxes in a
460 subduction zone. The ambiguity results from the curvature in $\Delta_{30} - N_2/^{36}\text{Ar}$ space. For
461 mixtures between air and MORB-like gases, mixing hyperbolae are associated with
462 considerable curvature. Most of the curvature occurs where $\Delta_{30} < \sim 4$ (Fig. 5A), such that for
463 any $\Delta_{30} > 4$, gas mixtures will inevitably be biased towards the $N_2/^{36}\text{Ar}$ of air. This means that
464 unless Δ_{30} of a mixed gas is almost indistinguishable from the high-temperature endmember,
465 which is a rare occurrence, the $N_2/^{36}\text{Ar}$ ratio remains poorly constrained by $\Delta_{30} - N_2/^{36}\text{Ar}$
466 extrapolations.

467

468 7.2 Constraints from $^{40}\text{Ar}/^{36}\text{Ar}$ ratios

469 A novel way to independently constrain $N_2/^{36}\text{Ar}$ ratios of high-temperature
470 endmembers is to plot Δ_{30} directly against $^{40}\text{Ar}/^{36}\text{Ar}$ (Fig. 6). In this space, samples from
471 intra-plate volcanism (Eifel and Yellowstone) show correlations which confirm that argon
472 and N_2 act essentially as geochemical pairs in hydrothermal fluids. Mixing curvatures are
473 defined by $[\text{}^{14}\text{N}^{14}\text{N}/^{36}\text{Ar}]_{\text{Mantle}}/[\text{}^{14}\text{N}^{14}\text{N}/^{36}\text{Ar}]_{\text{Air}}$. Taking the $N_2/^{36}\text{Ar}$ ratio for air-saturated
474 water and $^{40}\text{Ar}/^{36}\text{Ar}$ of both air (~ 300) and the plume endmembers ($\sim 30,000$ for Eifel,
475 $\sim 10,000$ for Yellowstone, see detail in Labidi et al., 2020), a simple data fit returns the
476 $N_2/^{36}\text{Ar}$ for the volcanic endmember. Overall, Yellowstone data are fit with a $N_2/^{36}\text{Ar}$
477 between $0.3_{-0.1}^{+0.2} \times 10^6$ and $1.0_{-0.4}^{+0.6} \times 10^6$ for the plume endmember (Fig. 6A). This is striking
478 because again, $N_2/^{36}\text{Ar}$ of individual samples are much closer to air (section 7.1). This

479 exercise would be valuable for fumaroles in a subduction zone, since it could distinguish
480 whether $N_2/^{36}Ar$ ratios for sub-arc source is 10^6 or 10^4 (Fig. 5A versus 5B). However, arc
481 fumaroles from Central America have atmospheric $^{40}Ar/^{36}Ar$ values even for near-zero Δ_{30}
482 values, so a spectrum of scenarios may account for the data. An endmember possibility is
483 that the sub-arc mantle sources have $^{40}Ar/^{36}Ar \sim 25,000$, i.e. the value of the upper mantle
484 away from direct slab influences (Moreira et al., 1998). To fit the vertical relationship in
485 figure 6, the required $N_2/^{36}Ar$ would have to be $\sim 10^8$ (Fig. 6B). In this case, the sub-arc
486 mantle would have to receive subducted nitrogen but no slab-derived argon at all, hence a
487 high $N_2/^{36}Ar$ and a MORB-like $^{40}Ar/^{36}Ar$. This may appear as unreasonable. In addition,
488 arguments based on $^3He/^{36}Ar$ suggest the addition of ^{36}Ar to sub-arc sources is actually
489 significant, which argues against a $N_2/^{36}Ar$ ratio of $\sim 10^8$ (Labidi et al., 2021). Instead, the
490 sub-arc mantle may be overwhelmed with atmospheric argon, with $^{40}Ar/^{36}Ar \sim 300$. In this
491 scenario, the $N_2/^{36}Ar$ of the arc source can be anything, but the vertical relationship on Fig.
492 6 is explained by volcanic argon having atmospheric $^{40}Ar/^{36}Ar$ ratios. This scenario is
493 consistent with the notion of subduction barrier for light noble gases (Moreira, 2013;
494 Moreira and Raquin, 2007; Staudacher and Allègre, 1988). It would incidentally confirm that
495 as opposed to Δ_{30} data, the Ar isotope systematic is not a strong tracer of air contamination
496 in arc regions, since high-temperature volatiles would have argon isotope compositions
497 similar to air.

498

499 **8. Determining the sources of N in the mantle**

500 A quantification of the flux of slab-derived N_2 to mantle sources is necessary for
501 understanding Earth's nitrogen cycle. Assuming that 3He subduction is negligible (Porcelli et

502 al., 2002), the combination of $N_2/{}^3\text{He}$ ratios and Δ_{30} values provides a particularly powerful
503 approach. For a discussion on ${}^3\text{He}/{}^{22}\text{Ne}$ and ${}^3\text{He}/{}^{36}\text{Ar}$ ratios, see Labidi et al., (2021). At
504 Yellowstone, the data require a $N_2/{}^3\text{He}$ endmember of 3×10^6 (Fig. 4), indistinguishable from
505 MORB. This $N_2/{}^3\text{He}$ estimate derived from Δ_{30} is the same as the lowest $N_2/{}^3\text{He}$ observed at
506 Yellowstone by Chiodini et al. (2012). The MORB-like $N_2/{}^3\text{He}$ ratio for the high ${}^3\text{He}/{}^4\text{He}$
507 Yellowstone plume, confirmed using Δ_{30} , is an important observation. Every ${}^3\text{He}$ -rich mantle
508 source may reflect a mixture of subducted and primordial reservoirs (Jackson et al., 2020)
509 especially for heavy noble gases (Ballentine et al., 2005; Parai and Mukhopadhyay, 2018).
510 Based on ${}^{15}\text{N}/{}^{14}\text{N}$ arguments, some have suggested the subducted components dominate the
511 N budget of plume sources (Barry and Hilton, 2016; Bekaert et al., 2021; Marty and Dauphas,
512 2003). Following Sano et al., (2001), the subducted components would likely show extremely
513 elevated $N_2/{}^3\text{He}$, perhaps as high as $\sim 10^{11}$. For subducted nitrogen to occur in the
514 Yellowstone source but still account for a MORB-like $N_2/{}^3\text{He}$ ratio of the mantle plume, the
515 primordial component would have to be characterized by an even lower $N_2/{}^3\text{He}$ ratios prior
516 to slab addition. In Labidi et al., (2020), mixtures involving slabs with $N_2/{}^3\text{He}$ of 10^{11} were
517 shown to require a primordial reservoir with $N_2/{}^3\text{He} \leq 2 \times 10^5$. A potential problem with
518 this view is that the $N_2/{}^3\text{He}$ of Yellowstone gases of $\sim 10^6$ would result from mixing two
519 extreme components in just the right proportions to yield convective mantle values. The
520 homogeneous $N_2/{}^3\text{He}$ of $\sim 10^6$ between MORB and a plume would have to result from chance.
521 A potentially simpler solution suggests that indistinguishable $N_2/{}^3\text{He}$ ratios for the
522 convective and deep mantle reflect that subduction is not a major player at all for nitrogen
523 in these reservoirs. The implications of the distinctive behaviors of nitrogen and heavy noble
524 gases during subduction are discussed elsewhere (Labidi, in revision in this issue). As

525 described above, we can use the sample with the lowest Δ_{30} reported by Labidi et al. (2020)
526 to provide a minimum $\delta^{15}\text{N}$ of $\sim+0.2\text{‰}$ for Yellowstone mantle, similar to the $\delta^{15}\text{N}$ of $\sim 0\text{‰}$
527 for the Yellowstone endmember reported by Chiodini et al. (2012). Given that the $\delta^{15}\text{N}$ of 0.2
528 ‰ is a minimum value, it becomes clear that the high $^3\text{He}/^4\text{He}$ mantle source of Yellowstone
529 features elevated $\delta^{15}\text{N}$ values yet with no resolvable N addition to the source (compared to
530 a MORB mantle). We tentatively suggest that $\delta^{15}\text{N} \sim 0\text{‰}$ in plumes may be indigenous to the
531 pristine mantle source rather than being the result of additions from descending slab
532 material (Fig. 7).

533 Literature data from Iceland and the Azores fumaroles may have to be revisited in
534 light of these findings. Fumaroles from these localities have $\text{N}_2/^3\text{He}$ values as low as $\sim 10^7$
535 that are associated with markedly negative $\delta^{15}\text{N}$ values (Marty et al., 1991; Caliro et al.,
536 2015). It is tempting to attribute $\delta^{15}\text{N} \leq -10\text{‰}$ to a hint of primordial nitrogen in plumes,
537 akin to the -20‰ to -47‰ $\delta^{15}\text{N}$ values exhibited by enstatite chondrites (Grady et al.,
538 1986). However, the $\text{N}_2/^3\text{He}$ ratios of $\sim 10^7$ are still far removed from the MORB-like mantle
539 endmember $\text{N}_2/^3\text{He}$ of $\sim 3 \times 10^6$ that we obtain from Δ_{30} - $\delta^{15}\text{N}$ systematics for the high $^3\text{He}/^4\text{He}$
540 mantle at Yellowstone. Mixing between a mantle gas ($\text{N}_2/^3\text{He} \sim 10^6$) and a relatively minute
541 amount of fractionated air ($\text{N}_2/^3\text{He} \sim 10^{11}$) can easily yield $\text{N}_2/^3\text{He}$ values $\sim 10^7$. A simple
542 mass balance shows that any mixing proportion involving more than 1% of air increases the
543 $\text{N}_2/^3\text{He}$ ratios to $\sim 10^7$ and overwhelms both Δ_{30} and $\delta^{15}\text{N}$ of the gas mixture air $\delta^{15}\text{N}$ values
544 (e.g., Figure 4). Should $\delta^{15}\text{N}$ of that particular air component be mass fractionated, as we
545 have shown is likely for air-derived nitrogen, $\text{N}_2/^3\text{He} \sim 10^7$ will be observed together with
546 low $\delta^{15}\text{N}$, leading us astray. We suggest this is the simplest explanation for the negative $\delta^{15}\text{N}$

547 signatures observed in Iceland (Marty et al., 1991) and the Azores (Caliro et al., 2015).
548 Instead of explaining very low $\delta^{15}\text{N}$ values for the high $^3\text{He}/^4\text{He}$ mantle as vestiges of an
549 enstatite chondrite source, we tentatively suggest that the high $^3\text{He}/^4\text{He}$ mantle may have a
550 $\delta^{15}\text{N}$ slightly elevated compared to MORB, with values around $\sim 0\text{‰}$ or slightly higher (Fig.
551 7).

552 Eifel gases display $\text{N}_2/{}^3\text{He}$ ratios of $1.2 (\pm 0.1) \times 10^7$ at near-zero Δ_{30} values (Fig. 4).
553 This is about a factor of 2–4 times the value for MORB, supporting the notion of nitrogen
554 addition to the Eifel mantle source. For gases from Central America, two-component mixing
555 curves define mixing between air with $\text{N}_2/{}^3\text{He} \sim 10^{11}$ and high-temperature gases with
556 $\text{N}_2/{}^3\text{He} \sim 10^8$ (Fig. 4). A $\text{N}_2/{}^3\text{He} \sim 10^8$, higher than MORB by two orders of magnitude, is
557 consistent with considerable nitrogen addition to sub-arc mantle sources (Labidi et al.,
558 2021). Samples at Poás have negative $\delta^{15}\text{N}$, values associated with low N_2/He ratios (Fischer
559 et al., 2002, Zimmer et al., 2004). This combination of geochemical features has been
560 interpreted as resulting from contributions of gases from the upper mantle, suggested to
561 account for $\sim 80\%$ of the vented N_2 (Fischer et al., 2002). However, these particular
562 fumaroles have atmospheric Δ_{30} signatures (Labidi et al., 2021), which argues against a
563 magmatic origin for N_2 . Here again, the simplest explanation for the low N_2/He ratios may
564 involve mixing between a mantle gas and air with fractionated $\delta^{15}\text{N}$ values. Importantly, the
565 Δ_{30} data mitigates the need to invoke substantial MORB-like nitrogen within the Central
566 American arc.

567 The new Δ_{30} data have been used to revisit the fluxes of nitrogen in arcs. Taking ^3He
568 fluxes from the literature and a newly-defined $\text{N}_2/{}^3\text{He}$ ratios of $\sim 10^8$, Labidi et al. (2021)
569 suggested N_2 outgassing fluxes are between 4.0×10^8 and 1.0×10^9 mol N_2/y . The revised

570 nitrogen outgassing fluxes are comparable to the subduction flux of nitrogen in this
571 subduction zone (Busigny et al., 2019). This suggests that in the Central American
572 subduction zone, the subduction and volcanic degassing fluxes of nitrogen are in balance
573 (Labidi et al., 2021), consistent with recent experimental work on the nitrogen partition
574 coefficient between slabs and fluids (Jackson et al., 2021; Mallik et al., 2018). This in turn
575 allows for the prospect that N₂ is quantitatively returned to the surface by degassing in
576 subduction zones, precluding a net delivery of nitrogen to the deep mantle (Fig. 7). If this
577 circumstance was typical globally and over geological timescales, it would explain the
578 apparent contradiction that air has a higher ¹⁵N/¹⁴N than the mantle whereas delivery of
579 isotopically heavy nitrogen in slabs to the mantle would predict the opposite over time.
580 Relative isolation of the mantle nitrogen from the surface seems to be required over
581 geological time scales (Labidi et al., 2020).

582

583

584 **9. Concluding remarks**

585 New Δ_{30} data, acquired with high-mass-resolution mass spectrometry, are a valuable
586 tool to constrain the behavior and sources of nitrogen in natural gas mixtures. In
587 hydrothermal fluids from various locations, the data are dominated by air-derived
588 components rather than by high-temperature volcanic volatiles. Using these data, we find
589 that air-derived components undergo isotope mass fractionations in hydrothermal systems.
590 This leads to the emanation of air-derived gases with negative $\delta^{15}\text{N}$ values and anomalously
591 low N₂/Ar and He/Ar ratios. This has consequence for the use of $\delta^{15}\text{N}$ and N₂/Ar as source
592 tracers in hydrothermal gases.

593 The new Δ_{30} data have allowed determinations of mantle $\delta^{15}\text{N}$, $\text{N}_2/^{36}\text{Ar}$, and $\text{N}_2/^{3}\text{He}$
594 ratios beneath Eifel and Yellowstone. For Eifel, the mantle $\text{N}_2/^{36}\text{Ar}$ and $\text{N}_2/^{3}\text{He}$ values are
595 slightly greater than the values for the MORB mantle. These values may reflect the addition
596 of nitrogen via subduction in the Eifel source. At Yellowstone, the mantle $\delta^{15}\text{N}$, $\text{N}_2/^{36}\text{Ar}$, and
597 $\text{N}_2/^{3}\text{He}$ values determined with Δ_{30} data yield important information about the high $^3\text{He}/^4\text{He}$
598 mantle. The $\text{N}_2/^{3}\text{He}$ elemental ratio is indistinguishable from the MORB mantle, and thus
599 inconsistent with N addition to the high $^3\text{He}/^4\text{He}$ mantle. The $\delta^{15}\text{N}$ value is indistinguishable
600 from 0‰, after appropriate correction for air contamination. The new Δ_{30} data show that
601 suggestions of a high $^3\text{He}/^4\text{He}$ mantle with very negative $\delta^{15}\text{N}$ values are not warranted.
602 Instead, the observed low $\delta^{15}\text{N}$ values are the result of $^{15}\text{N}/^{14}\text{N}$ fractionation in hydrothermal
603 systems. Air-like $\delta^{15}\text{N}$ values with MORB-like $\text{N}_2/^{3}\text{He}$ ratios appear to be a fundamental
604 observation that constrains the origin of volatiles in the high $^3\text{He}/^4\text{He}$ mantle. More work is
605 needed on ^3He rich hotspots. Iceland hosts many fumaroles and geothermal wells where light
606 noble gases have features associated with the plume mantle (Füri et al., 2010). Acquisition
607 of Δ_{30} measurements for these fumaroles will be important. The only Δ_{30} measurements of
608 nitrogen from Icelandic fluids, reviewed here, have identified no non-atmospheric N_2 . Future
609 attempts to identify high-temperature N_2 there, if successful, would be useful for
610 determining whether the low $\text{N}_2/^{3}\text{He}$ that characterizes the Yellowstone plume is a global
611 signature of the primordial mantle.

612 Plots featuring $^{40}\text{Ar}/^{36}\text{Ar}$ versus Δ_{30} are helpful when mantle endmembers have a known,
613 elevated, $^{40}\text{Ar}/^{36}\text{Ar}$ ratio, as in the cases of plumes. For those cases, measured $\text{N}_2/^{36}\text{Ar}$ on
614 individual samples are ambiguous regarding the source, but the approach of fitting mixing
615 curves to the data (e.g., Fig. 6) affords a determination of $\text{N}_2/^{36}\text{Ar}$. The approach is sensitive

616 to the $N_2/^{36}Ar$ ratios used for air components. When the $^{40}Ar/^{36}Ar$ of a mantle source is
617 unknown (e.g., a subduction zone), the Δ_{30} data support the concept of sub-arc mantle
618 sources entirely dominated by air-derived argon.

619 New Δ_{30} data provide novel constraints on the fate of nitrogen in subduction zones.
620 The sub-arc source from the warm subduction zone in Central America is shown to have
621 elevated $N_2/^{3}He$ by orders of magnitude compared to the MORB mantle. This shows
622 considerable addition of N_2 to sub-arc sources. Revised fluxes in the Central American
623 subduction zone are based on $N_2/^{3}He$ that in turn derive from the analysis of Δ_{30} data. The
624 derived fluxes suggest that this margin is a subduction barrier for N_2 . Using fluxes
625 determined on warm subduction zones may be more relevant to the deep time than those
626 characterizing cold subduction zones. The true influence of subduction on mantle volatiles
627 through time warrants revision based on these results.

628

629

630 **Appendix A: Mixing loops**

631 The concept of isotope clumping uses the stochastic distribution of isotopologues as a reference frame. Mixing in this
632 reference frame can be highly non-linear. We illustrate mixing with N_2 gases with different bulk isotopic composition, gas
633 1 with $\delta^{15}N$ of -200‰ , and gas 2 with a $\delta^{15}N$ of $+100\text{‰}$. For this exercise, both gases will be assigned a stochastic
634 distribution of isotopologues, i.e. $\Delta_{30} = 0\text{‰}$. The stochastic relative abundance of $^{15}N^{15}N$ in gas 1 is the square of the singly-
635 substituted value, treating relative abundances as probabilities:

636

$$637 \quad x(^{15}N^{15}N)_{\text{gas1}} = x(^{15}N)^2 = 8.50 \times 10^{-6}, \quad (1)$$

638

639 where $x(^{15}N^{15}N)_{\text{gas1}}$ is the mole fraction of the $^{15}N^{15}N$ isotopologue in gas 1, and so forth. Similarly, the stochastic relative
640 abundance of $^{15}N^{15}N$ in gas 2 is:

$$641 \quad x(^{15}N^{15}N)_{\text{gas2}} = x(^{15}N)^2 = 1.60 \times 10^{-5}. \quad (2)$$

642

643 We calculate the expected stochastic abundance of $^{15}N^{15}N$ for a 50:50 mixture of these two gases from the bulk $^{15}N/^{14}N$
644 ratio in the usual way, as the square of the bulk isotopic concentration

645

646
$$\chi(^{15}\text{N}^{15}\text{N})_{50:50,\text{stochastic}} = \chi(^{15}\text{N})^2 = 1.20 \times 10^{-5}. \quad (3)$$

647
 648 However, simple mixing between these two gases does not involve bond rupture. Since molecules retain their original
 649 bond ordering, the physical mixture has an observed fractional abundance of $^{15}\text{N}^{15}\text{N}$ different from that in equation 3.

650 The relative concentration of $^{15}\text{N}^{15}\text{N}$ for the physical mixture is

651
 652
$$\frac{1}{2} \chi(^{15}\text{N}^{15}\text{N})_{\text{gas1}} + \frac{1}{2} \chi(^{15}\text{N}^{15}\text{N})_{\text{gas2}} = 1.23 \times 10^{-5} \quad (4)$$

653
 654 Comparing the measured value from Equation (4) with the predicted stochastic value from Equation (3) leads to an
 655 apparent Δ_{30} value greater than zero:

656
 657
$$\Delta_{30} = 10^3 (1.23 \times 10^{-5} / 1.20 \times 10^{-5} - 1) = 25 \text{ ‰} \quad (5)$$

658
 659 The mixing between these two gases results in a Δ_{30} value even higher than air. This effect may prove important for the
 660 interpretation of data on other planets or in the interstellar medium where cold chemistry will cause $^{15}\text{N}/^{14}\text{N}$ ratios to vary
 661 by extreme magnitudes in terrestrial terms (Füri and Marty, 2015). However on Earth, mixing between $^{15}\text{N}/^{14}\text{N}$ ratios
 662 differing by hundreds of per mil is unrealistic. Mixing between two gases with $\delta^{15}\text{N}$ of -10‰ and $+10\text{‰}$ encompasses the
 663 vast majority of likely scenarios on Earth. In this case, the mixing produces negligible effects. At a 50:50 mixture of gases
 664 with $\delta^{15}\text{N}$ values of -10‰ and $+10\text{‰}$ and Δ_{30} of 0‰ , results in Δ_{30} value of 0.1‰ . In other words, in mixing scenarios
 665 where $^{15}\text{N}/^{14}\text{N}$ ratios vary by less than $\sim 40\text{‰}$, the induced Δ_{30} values deviate from endmember values by at most tenths
 666 of per mil. We conclude that mixing in the Δ_{30} - $\delta^{15}\text{N}$ space where variations in $\delta^{15}\text{N}$ are less than many tens of per mil (e.g.,
 667 Fig. 2) produces linear trends.

668
 669 **Appendix B: Combinatorial effects**

670 The combinatorial effect is an artifact of the use of the stochastic reference frame to characterize enrichments and
 671 depletions of multiply-substituted isotopologues signatures (Taenzer et al., 2020; Yeung, 2016; Yeung et al., 2015; Young
 672 et al., 2017). It can arise where more than one isotopic pool of an element contributes to the formation of the multiply-
 673 substituted molecules of interest. The most succinct description of the effect is that the analyst can only measure the
 674 arithmetic mean of those distinct pools, in the form of the product molecules, whereas the actual abundance of the multiply-
 675 substituted, or “clumped”, species is the result of the geometric mean. Here we dispense with the possibility that the
 676 difference between air and other reservoirs of N_2 might be the result of this effect.

677 We might imagine that N_2 molecules are constructed from two different sources of nitrogen with distinct $^{15}\text{N}/^{14}\text{N}$
 678 ratios, $^{15}\text{R}_1$ and $^{15}\text{R}_2$. Such a circumstances may obtain in the construction of O_2 molecules during photosynthesis, for
 679 example (Yeung et al., 2015, Yeung 2016), or when adding H to CH_3 to form methane (Taenzer et al., 2020). In the case of
 680 the formation of a molecule with a stochastic abundance of $^{15}\text{N}^{15}\text{N}$, but in which $^{15}\text{R}_1$ and $^{15}\text{R}_2$ contribute to the two different
 681 positions in the homonuclear diatomic N_2 , the ratio of $^{15}\text{N}^{15}\text{N}$ to $^{14}\text{N}^{14}\text{N}$, given as the ratio of their mole fractions,
 682 $\chi^{15}\text{N}^{15}\text{N}/\chi^{14}\text{N}^{14}\text{N}$, must be the probability of $^{15}\text{R}_1$ and $^{15}\text{R}_2$ occurring in the same molecule, or $^{15}\text{R}_1 \times ^{15}\text{R}_2$, so in reality
 683 $\chi^{15}\text{N}^{15}\text{N}/\chi^{14}\text{N}^{14}\text{N} = ^{15}\text{R}_1 \times ^{15}\text{R}_2$. However, the analyst has no *a priori* knowledge about the ratios $^{15}\text{R}_1$ and $^{15}\text{R}_2$. Therefore,
 684 when reporting Δ_{30} value for this gas, the only recourse available is to use the bulk $^{15}\text{N}/^{14}\text{N}$ of the molecules themselves to

685 derive the stochastic value (the denominator in Δ_{30} values). This bulk ratio is the arithmetic mean of the ratios $^{15}\text{R}_1$ and
 686 $^{15}\text{R}_2$, or $(^{15}\text{R}_1+^{15}\text{R}_2)/2$. The resulting expression for the “observed” Δ_{30} is

$$687 \quad \Delta_{30} = \frac{x^{15}\text{N}^{15}\text{N} / x^{14}\text{N}^{14}\text{N}}{\left(\frac{^{15}\text{R}_1 + ^{15}\text{R}_2}{2}\right)^2} - 1$$

688 (6)

689 whereas the actual, “true” value should be
 690

$$691 \quad \Delta_{30} = \frac{x^{15}\text{N}^{15}\text{N} / x^{14}\text{N}^{14}\text{N}}{^{15}\text{R}_1 \ ^{15}\text{R}_2} - 1$$

692 (7)

693 where for convenience we have omitted the factor of 10^3 that puts the values in per mil. As an illustration, we consider the
 694 extreme case where the isotopic compositions of the two nitrogen pools differ by 100 ‰, a difference much greater than
 695 found among natural geochemical or biogeochemical reservoirs. In this example, $^{15}\text{R}_1=1.100 \times ^{15}\text{R}_2$, or $\delta^{15}\text{N}_{(1)}= 100\text{‰}$ and
 696 $\delta^{15}\text{N}_{(2)}= 0\text{‰}$. In addition, for convenience, we stipulate that the “clumping” in this gas is 0, meaning that there is no excess
 697 in $^{15}\text{N}^{15}\text{N}$ relative to stochastic. Using the average natural abundances of ^{15}N and ^{14}N to define $^{15}\text{R}_2$, 0.00364 and 0.99636,
 698 respectively, we have $^{15}\text{R}_2 = 0.003653$, and the stochastic abundance of $^{15}\text{N}^{15}\text{N}$ in the N_2 composed of one atom from
 699 reservoir 1 and the other from reservoir 2 is $x^{15}\text{N}^{15}\text{N}/x^{14}\text{N}^{14}\text{N}= ^{15}\text{R}_1 \times ^{15}\text{R}_2 = 1.46812 \times 10^{-5}$. Using Equation (7) to calculate
 700 Δ_{30} , we obtain 0, as expected. However, the analyst cannot apply Equation (8) because there is nothing to indicate that the
 701 two nitrogen atoms represent two distinct isotopic pools; the values of $^{15}\text{R}_1$ and $^{15}\text{R}_2$ are unknowable. Forced to use
 702 Equation (6), the analyst obtains a Δ_{30} value of -2.27‰ for this stochastic gas. This is the spurious negative Δ value caused
 703 by the combinatorial effect. For more typical differences in $\delta^{15}\text{N}$ among relevant reservoirs of tens of per mil at most, these
 704 effects are on the order of a tenth of ‰ or less, and then only if N_2 is constructed from nitrogen atoms from two distinct
 705 isotopic pools. The combinatorial effect is not a factor in the applications described in this review, and it cannot explain the
 706 $\sim 19 \text{‰}$ enrichment in $^{15}\text{N}^{15}\text{N}$ in air.

707
 708
 709
 710

711 **Appendix C: evidence against $^{15}\text{N}^{15}\text{N}$ bond re-ordering**

712 Atmospheric N_2 , with $\Delta_{30} \sim 19\text{‰}$, may be kept at relatively high temperatures within heated hydrothermal systems.
 713 This could re-order nitrogen to a near-stochastic distribution of the doubly-substituted isotopologue $^{15}\text{N}^{15}\text{N}$, leading to N_2
 714 with $\Delta_{30} = 0$. Partial or total bond re-ordering of atmospheric signatures is however considered unlikely, on the basis of
 715 experimental evidence and circumstantial observation in nature.

716 Pure N_2 at a pressure of 0.1 bar was heated at 800 °C for between 1 and 69 days. The heated N_2 yielded average Δ_{30}
 717 of 19.2 ± 0.2 indistinguishable from the starting Δ_{30} composition of air. In a second set of experiments, N_2 was in contact with
 718 2 grams of basalt powder (< 68 microns mesh), as a ways to increase the potential reaction surfaces between gases and
 719 solids with rock material that may be present at depths in natural hydrothermal systems. The gas+powder mixture was
 720 heated at 800 °C for up to 38 days. In these experiments N_2 yielded average Δ_{30} of 19.0 ± 0.2 .

721 The evidence against re-ordering in heating experiments is corroborated by circumstantial observations in nature.
722 Gases vented at 400 °C in el Salvador, up to 212 °C in Iceland, and 200 °C in Hawaii are among the samples analyzed for Δ_{30}
723 with the highest venting temperatures. At these temperature, bond re-ordering would result equilibrium Δ_{30} value below
724 0.3‰ (Yeung et al., 2017). However, nitrogen from these samples have high Δ_{30} value of 15.5 ± 0.3 ‰, 18.6 ± 0.8 ‰ and
725 18.2 ± 0.4 ‰ respectively. Those are near atmospheric signatures which argues against the erasure of $^{15}\text{N}^{15}\text{N}$ atmospheric
726 excesses. A number of other gases vented at ~ 100 – 150 °C show strictly atmospheric Δ_{30} values.

727 Last, we note that re-ordering would cause vertical trends in plots of Δ_{30} vs $\delta^{15}\text{N}$ on Figure 4, as it would only affect
728 Δ_{30} values, not the bulk $^{15}\text{N}/^{14}\text{N}$ ratios. This is not observed; $^{15}\text{N}/^{14}\text{N}$ ratios correlate with Δ_{30} values. These correlations
729 require mixing processes. The absence of Δ_{30} re-ordering on timescales relevant to hydrothermal systems allow
730 extrapolation to $\Delta_{30} \sim 0$ ‰ to distinguish melt-derived volatiles from atmospheric components.

731

732

733

734

735

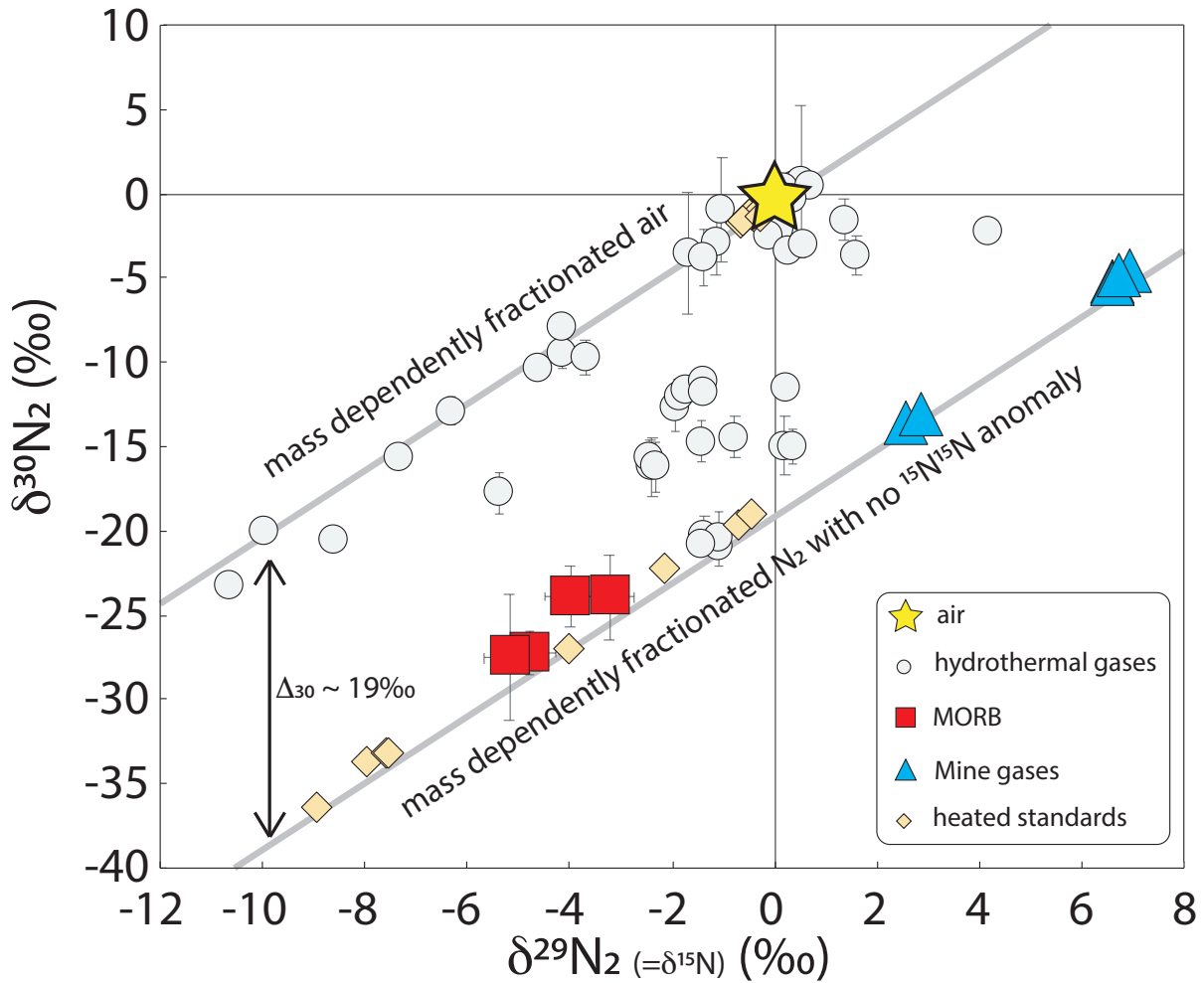
736

737

738

739

740 **Captions**



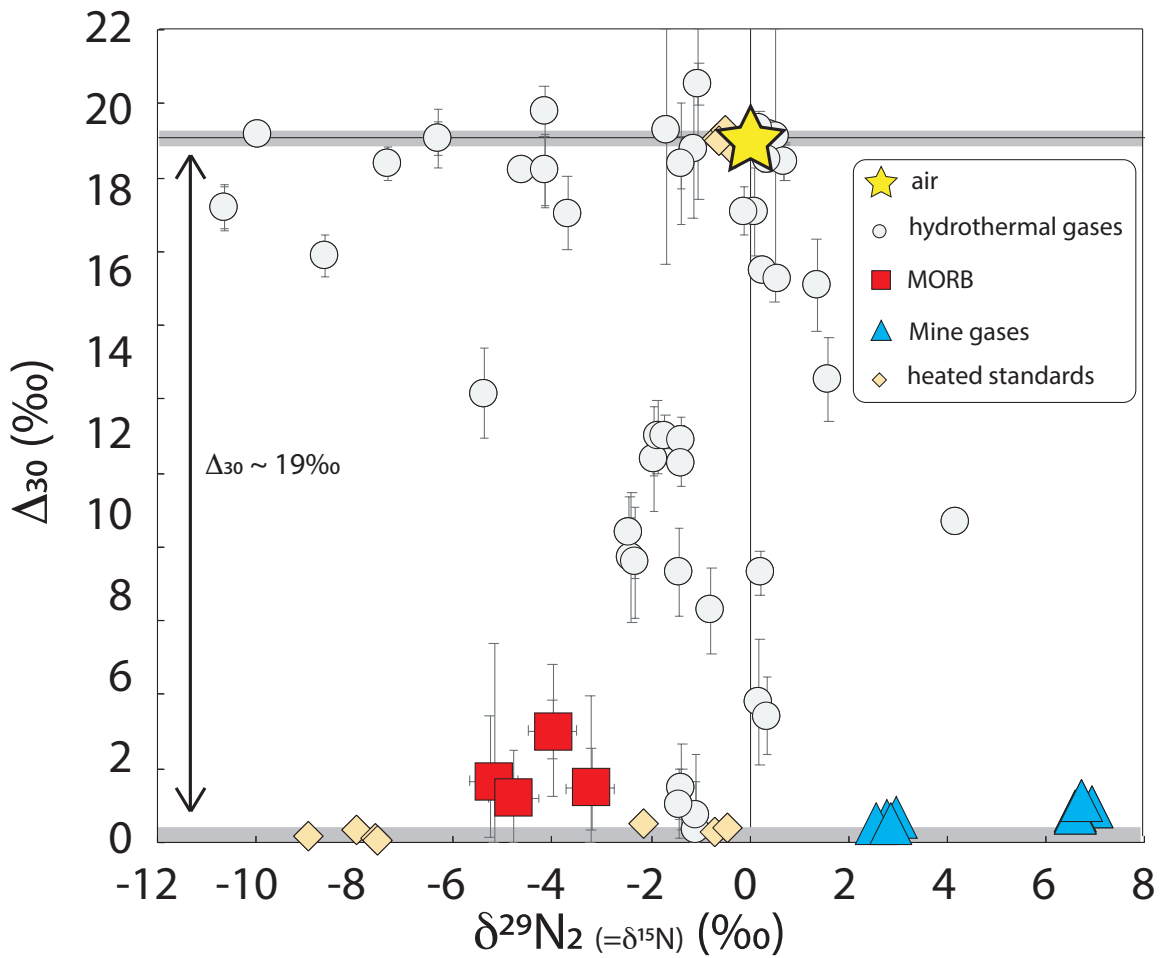
741

742 **Figure 1: Isotopic composition of N_2 from natural samples and laboratory experiments for $\delta^{30}\text{N}_2$ versus $\delta^{29}\text{N}_2$.** Mass-
 743 dependent fractionation curves for air and high-temperature stochastic N_2 are shown. Data are from Yeung et al. (2017),
 744 Labidi et al., (2020), and Labidi et al., (2021). Detail on heated gases can be found in Yeung et al., (2017). Briefly, heated
 745 gases in the absence of a catalyst show un-equilibrated Δ_{30} values, so they plot near air. Only heated gases in the presence
 746 of strontium nitride show re-ordered, stochastic distributions of $^{15}\text{N}^{15}\text{N}$. Most data on natural samples are from Labidi et
 747 al., (2020, 2021). Natural samples are dominated by hydrothermal vents, but also include mid-ocean ridge basalts and mine
 748 gases.

749

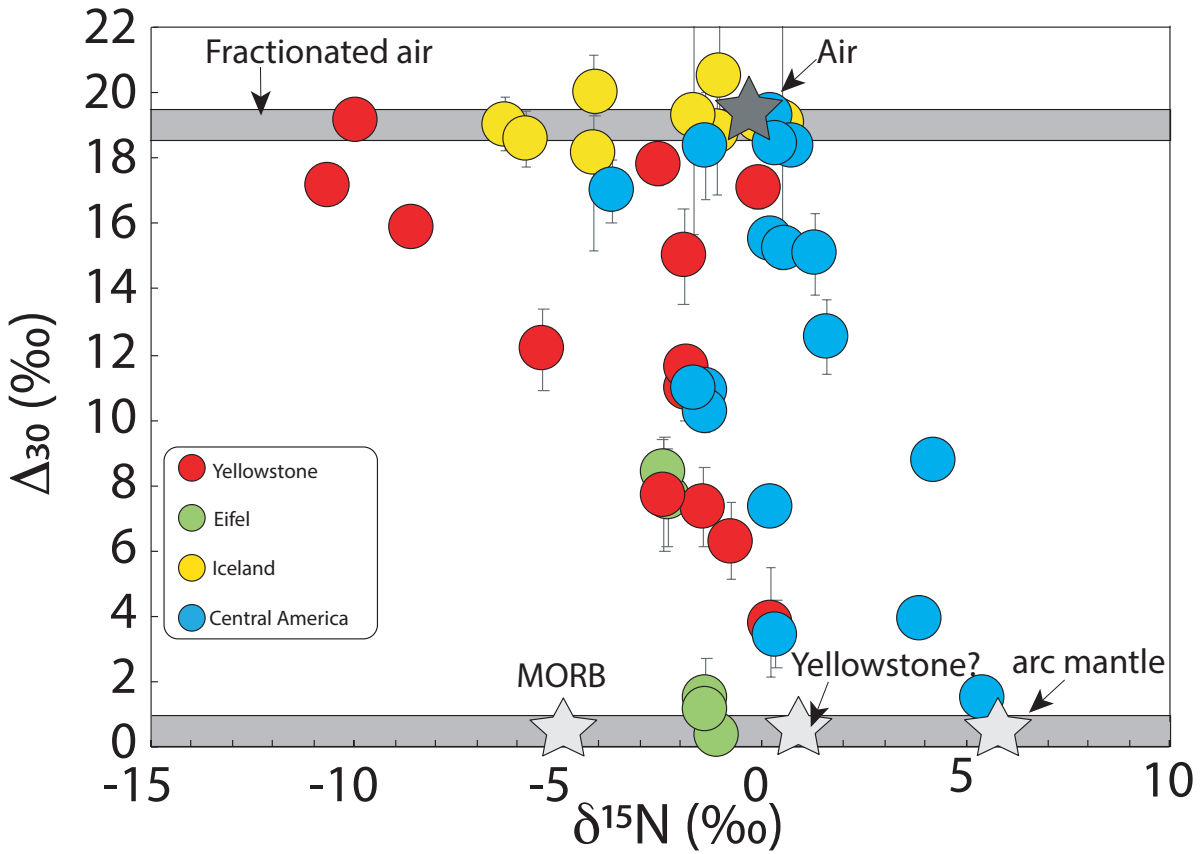
750

751



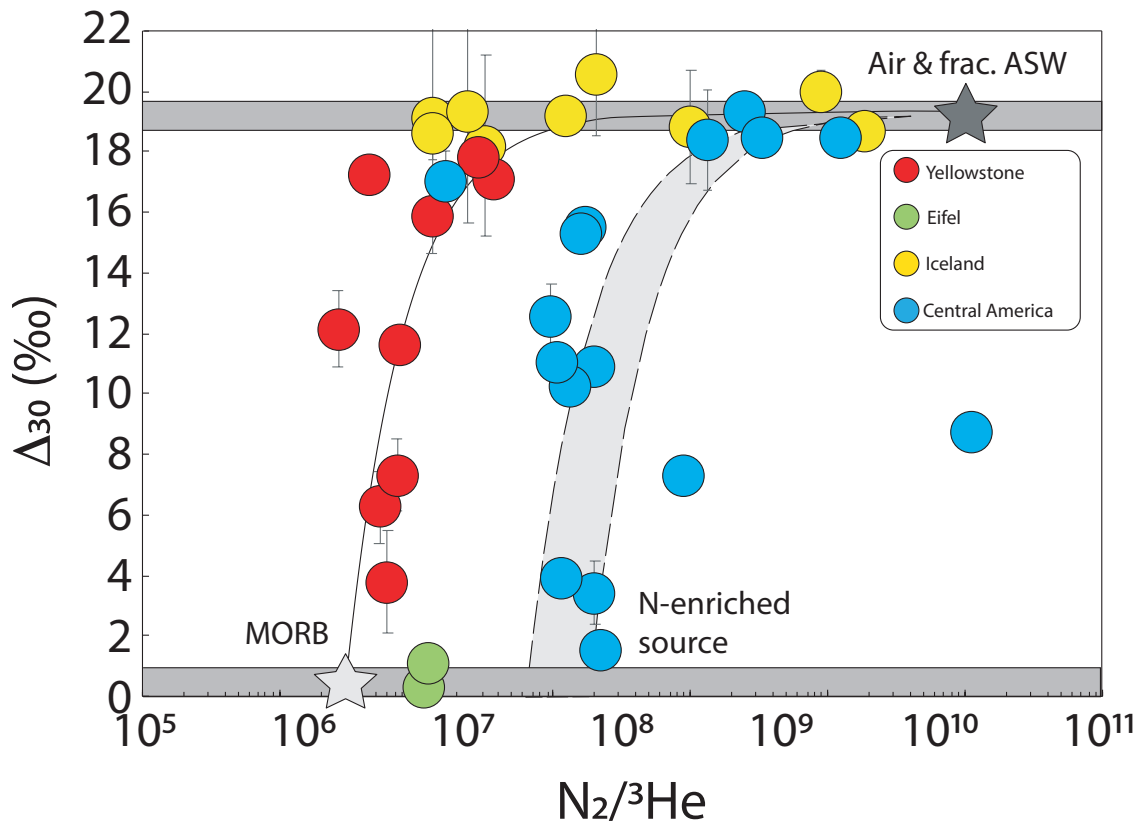
752
753
754
755
756
757
758

Figure 2: Isotopic composition of N_2 from natural samples and laboratory experiments for Δ_{30} versus $\delta^{15}\text{N}$. A $\sim 19\text{‰}$ offset is observed between air and stochastic gases. Hydrothermal samples show variable $\delta^{15}\text{N}$ and Δ_{30} . The Δ_{30} variation reflects mixing between stochastic and air-derived N_2 . Importantly, negative $\delta^{15}\text{N}$ are almost exclusively associated with air that underwent N isotope fractionation, as shown by atmospheric Δ_{30} values.



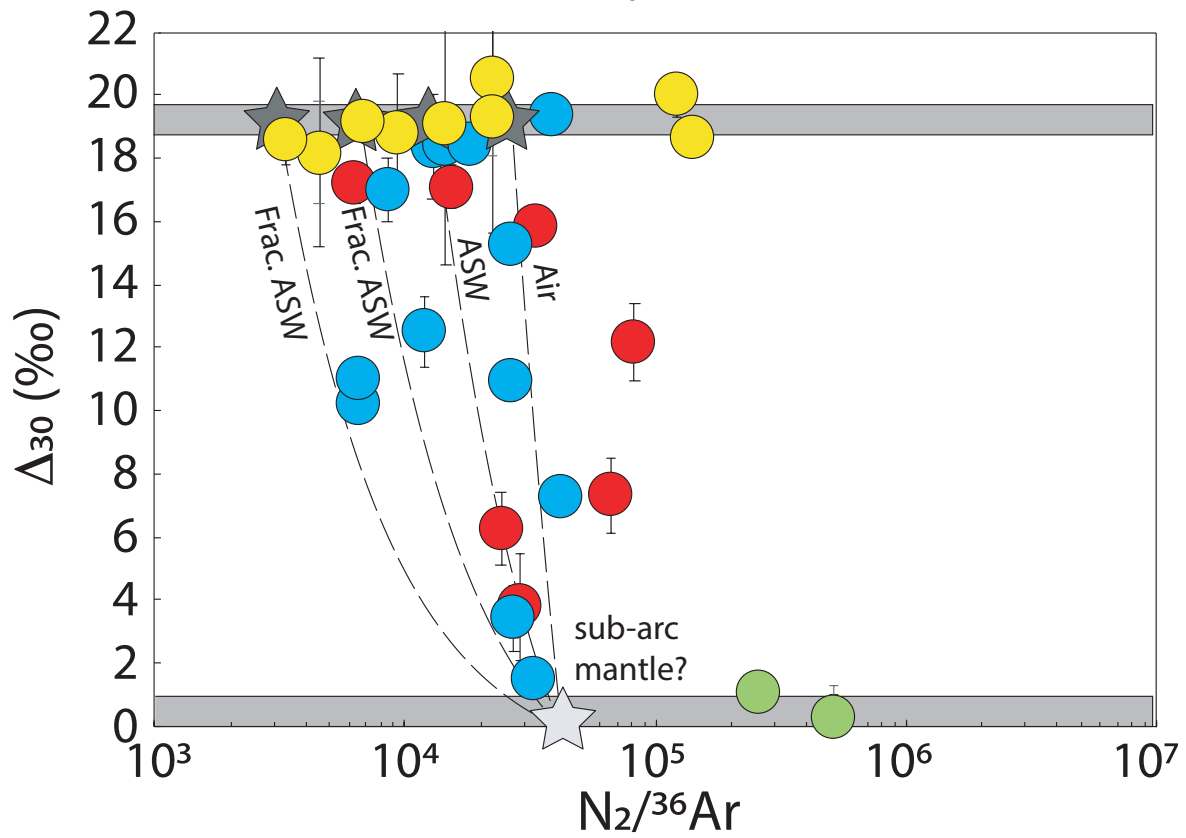
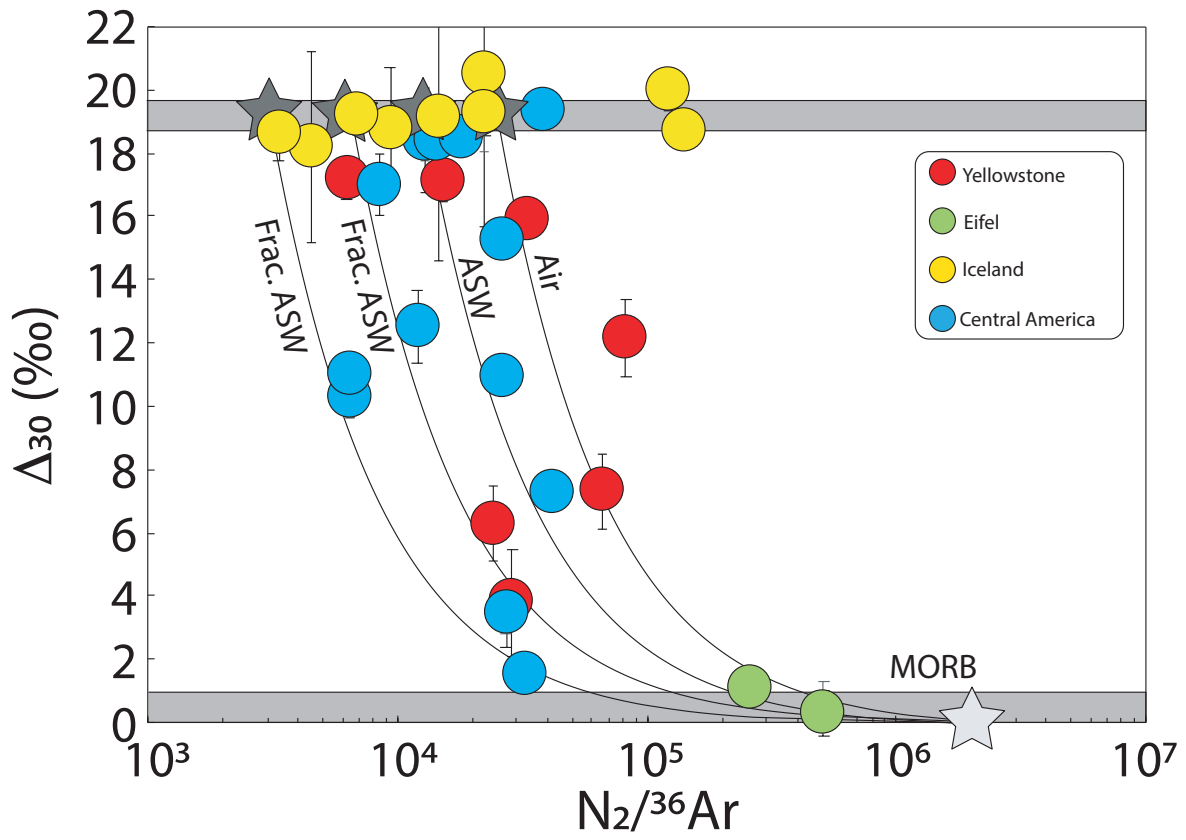
759
 760
 761
 762
 763
 764
 765
 766

Figure 3: **nitrogen isotopic data of volcanic discharges from Iceland, Eifel, Yellowstone, and Central America**
 Variable Δ_{30} values establish that the samples incorporate variable amounts of atmospheric nitrogen. At an air Δ_{30} value, variable $\delta^{15}\text{N}$ reflect a mass-dependent isotope fractionation associated with hydrothermal degassing. The high-temperature components are identified by attempting at extrapolating the trends. For Yellowstone, the scatter makes it particularly challenging, but the data appear consistent with a near-zero $\delta^{15}\text{N}$ value for the high-T endmember.

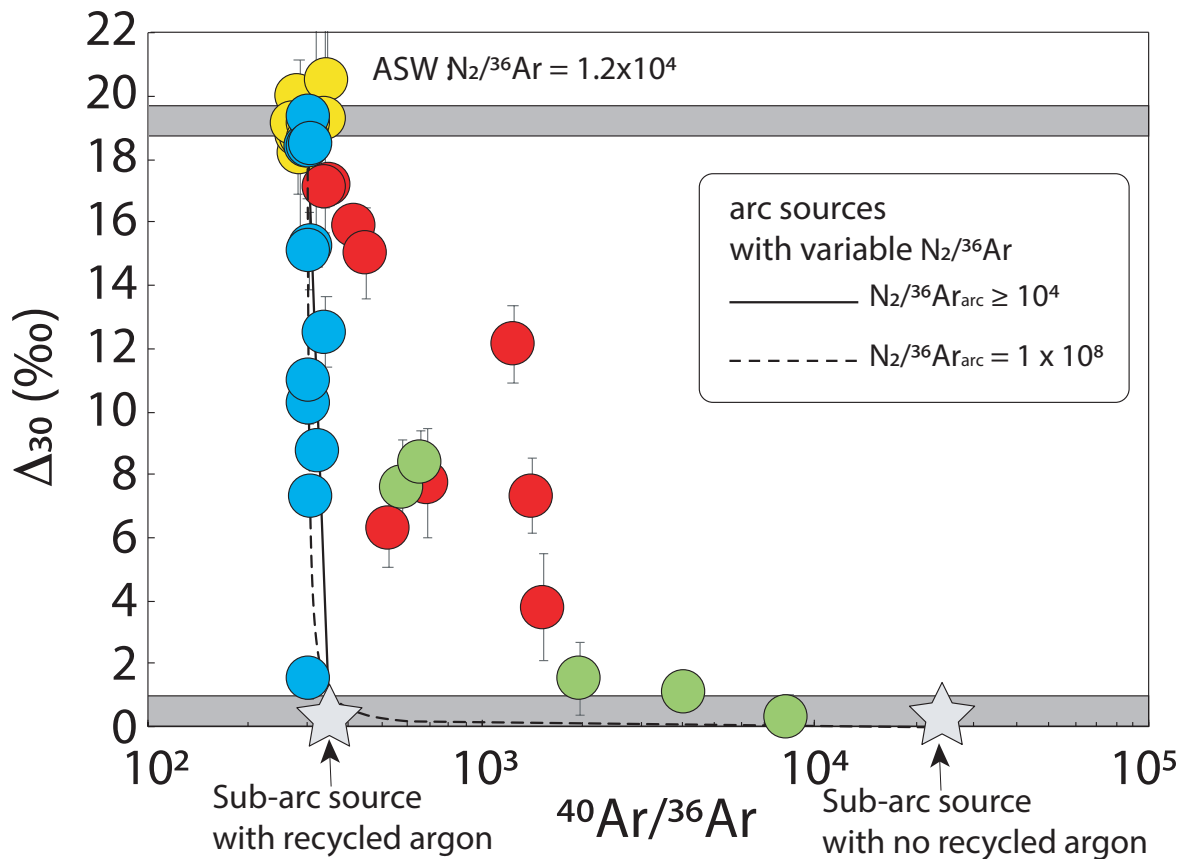
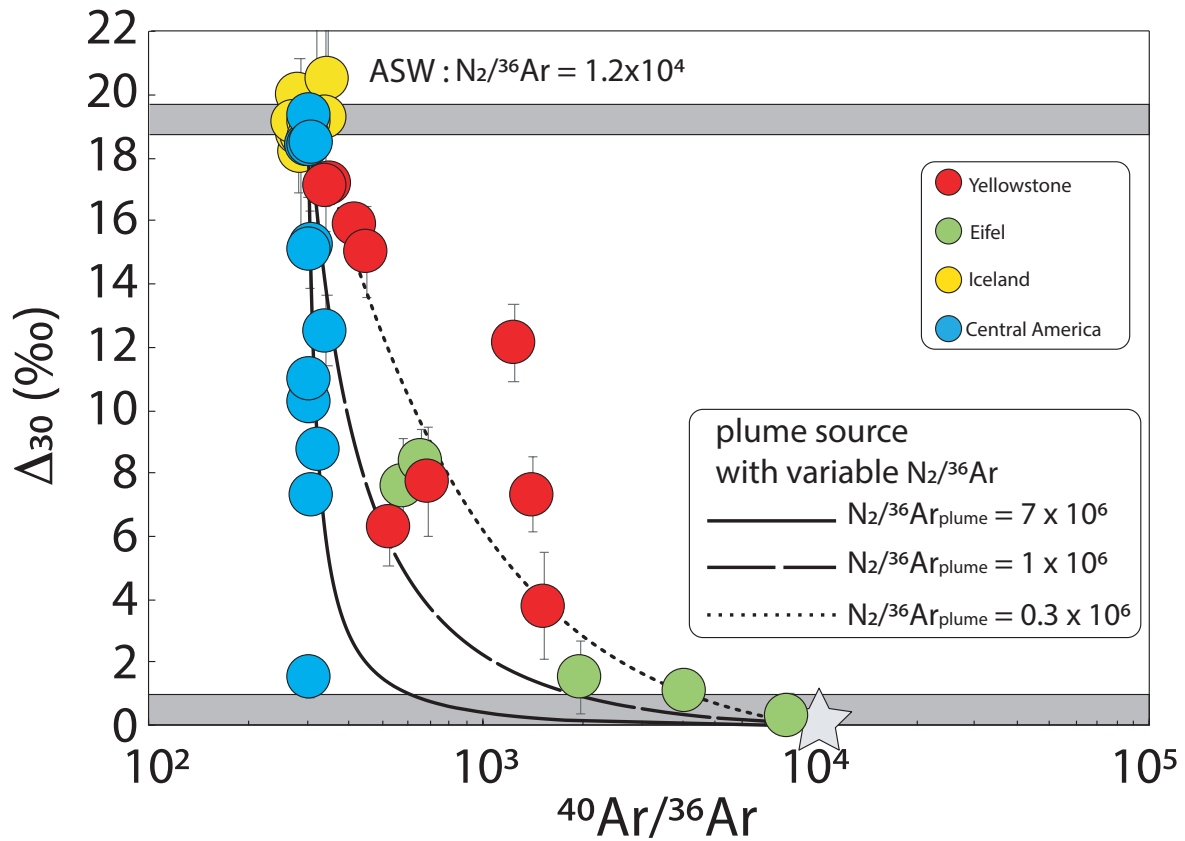


767
768
769
770
771

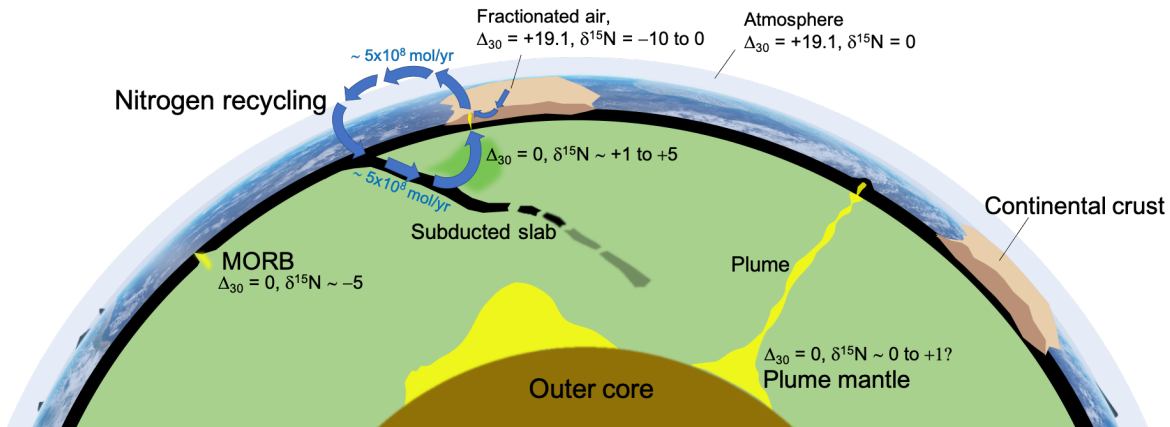
Figure 4: **Measured $N_2/{}^3He$ ratios versus Δ_{30} values.** Mixing lines are shown for mixtures between air and high temperature components. Because the solubility of N_2 and He are indistinguishable in waters at most hydrothermal temperatures (Ballentine et al., 2002), air, air-saturated water (ASW) and fractionated ASW all have indistinguishable $N_2/{}^3He$ ratios.



773 Figure 5: **Measured $N_2/^{36}Ar$ ratios versus Δ_{30} values.** Panel A and B are identical geochemical spaces with distinct mixing
774 scenarios, constructed both in order to explain the Yellowstone and Central American data. In Panel A, mixing lines are between
775 a MORB component and variably fractionated atmospheric components, including air, air-saturated water (ASW), and degassed
776 water. In Panel B, mixing lines are between a hypothetical mantle wedge endmember and the same atmospheric components
777 than in panel A.
778



780 **Figure 6 The relationship between nitrogen Δ_{30} and argon isotopes in volcanic gases**
 781 Δ_{30} and $^{40}\text{Ar}/^{36}\text{Ar}$ ratios are shown for Iceland, Yellowstone, Eifel and central America gases. Panel A and B are identical
 782 geochemical spaces with distinct mixing scenarios. Panel A aims at accounting for the Yellowstone data. Mixing lines are between
 783 ASW and a hypothetical plume endmember with $^{40}\text{Ar}/^{36}\text{Ar}$ ratio of 10,000. Variable $\text{N}_2/^{36}\text{Ar}$ ratios for the plume component cause
 784 variable curvatures in the mixing relationships. Panel B aims at account for the Central American dataset. Mixing lines are
 785 between ASW and a hypothetical mantle wedge endmembers with variable $^{40}\text{Ar}/^{36}\text{Ar}$ ratios.
 786
 787



788 **Figure 7 Cartoon representing various processes and reservoirs constrained by $^{15}\text{N}^{15}\text{N}$ data.**
 789 Not to scale. A section of Earth with the core, the mantle, the continental and oceanic crust, and the atmosphere are shown. A
 790 slab is shown to enter subduction. Air is the only reservoir with N_2 associated with a $^{15}\text{N}^{15}\text{N}$ anomaly of $\sim 19\text{‰}$. All other sources
 791 of N_2 have $\Delta_{30} \sim 0\text{‰}$. The slab hosts nitrogen fixed as NH_4^+ (Busigny et al., 2019 and references therein) so no Δ_{30} values are
 792 defined; Δ_{30} is only relevant for N_2 molecules. Upon partial melting of a mantle source, magmatic N_2 would form with a Δ_{30} of
 793 0‰ . The high-T N_2 is then contributed to hydrothermal systems in the sub-surface by near-quantitative magmatic degassing. Air
 794 circulation in the sub-surface allows air-saturated waters to undergo degassing, and subsequent gas release with fractionated
 795 compositions. Plume data require a mantle source with a $\delta^{15}\text{N} \sim 0\text{‰}$, from the study of Yellowstone, in agreement with Chiodini
 796 et al., (2012). No enstatite-like $\delta^{15}\text{N}$ signatures appear to be required by the data in the Yellowstone plume source. The plume
 797 source has a $\text{N}_2/^{3}\text{He}$ similar to the MORB mantle, which could challenge the notion of nitrogen addition to plume sources with
 798 elevated $^3\text{He}/^4\text{He}$ ratios (Labidi et al., 2020). The arc sources underneath the central American arc are even more enriched in
 799 $\delta^{15}\text{N}$, with values up to $+5\text{‰}$ according to $^{15}\text{N}^{15}\text{N}$ data. There, elevated $\text{N}_2/^{3}\text{He}$ across the entire arc require the overwhelming
 800 addition of surface-derived N to sub-arc sources. Recalculated fluxes suggest that, in that one subduction zone, ingassing and
 801 outgassing fluxes are matching within uncertainties (Labidi et al., 2021).
 802
 803
 804
 805
 806
 807
 808
 809
 810
 811

812 References

813
 814 Ader, M., Thomazo, C., Sansjofre, P., Busigny, V., Papineau, D., Laffont, R., Cartigny, P., Halverson, G.P., 2016. Interpretation of the nitrogen
 815 isotopic composition of Precambrian sedimentary rocks: Assumptions and perspectives. *Chem. Geol.* 429, 93–110.
 816 Ballentine, C.J., Burgess, R., Marty, B., 2002. Tracing fluid origin, transport and interaction in the crust. *Rev. Mineral. geochemistry* 47,
 817 539–614.
 818 Ballentine, C.J., Marty, B., Lollar, B.S., Cassidy, M., 2005. Neon isotopes constrain convection and volatile origin in the Earth's mantle.

819 Nature 433, 33–38.

820 Barry, P.H., Hilton, D.R., 2016. Release of subducted sedimentary nitrogen throughout Earth’s mantle. *Geochemical Perspect. Lett.* 2, 148–
821 159. <https://doi.org/http://dx.doi.org/10.7185/geochemlet.1615>

822 Bebout, G.E., Fogel, M.L., 1992. Nitrogen-isotope compositions of metasedimentary rocks in the Catalina Schist, California: implications
823 for metamorphic devolatilization history. *Geochim. Cosmochim. Acta* 56, 2839–2849.

824 Bekaert, D.V., Turner, S.J., Broadley, M.W., Barnes, J.D., Halldórsson, S.A., Labidi, J., Wade, J., Walowski, K.J., Barry, P.H., 2021. Subduction-
825 Driven Volatile Recycling: A Global Mass Balance. *Annu. Rev. Earth Planet. Sci.* 49.

826 Boudoire, G., Rizzo, A.L., Arienzo, I., Di Muro, A., 2020. Paroxysmal eruptions tracked by variations of helium isotopes: inferences from
827 Piton de la Fournaise (La Réunion island). *Sci. Rep.* 10, 1–16.

828 Busigny, V., Cartigny, P., Philippot, P., 2011. Nitrogen isotopes in ophiolitic metagabbros: A re-evaluation of modern nitrogen fluxes in
829 subduction zones and implication for the early Earth atmosphere. *Geochim. Cosmochim. Acta* 75, 7502–7521.
830 <https://doi.org/10.1016/j.gca.2011.09.049>

831 Busigny, V., Cartigny, P., Philippot, P., Ader, M., Javoy, M., 2003. Massive recycling of nitrogen and other fluid-mobile elements (K, Rb, Cs,
832 H) in a cold slab environment: evidence from HP to UHP oceanic metasediments of the Schistes Lustrés nappe (western Alps,
833 Europe). *Earth Planet. Sci. Lett.* 215, 27–42. [https://doi.org/10.1016/s0012-821x\(03\)00453-9](https://doi.org/10.1016/s0012-821x(03)00453-9)

834 Caliro, S., Viveiros, F., Chiodini, G., Ferreira, T., 2015. Gas geochemistry of hydrothermal fluids of the S. Miguel and Terceira Islands,
835 Azores. *Geochim. Cosmochim. Acta* 168, 43–57.

836 Cartigny, P., Jendrzejewski, N., Pineau, F., Petit, E., Javoy, M., 2001. Volatile (C, N, Ar) variability in MORB and the respective roles of
837 mantle source heterogeneity and degassing: the case of the Southwest Indian Ridge. *Earth Planet. Sci. Lett.* 194, 241–257.

838 Chiodini, G., Caliro, S., Lowenstern, J.B., Evans, W.C., Bergfeld, D., Tassi, F., Tedesco, D., 2012. Insights from fumarole gas geochemistry on
839 the origin of hydrothermal fluids on the Yellowstone Plateau. *Geochim. Cosmochim. Acta* 89, 265–278.
840 <https://doi.org/10.1016/j.gca.2012.04.051>

841 Clayton, R.N., Mayeda, T., 1984. The oxygen isotope record in Murchison and other carbonaceous chondrites. *Earth Planet. Sci. Lett.* 67,
842 151–161.

843 Dauphas, N., Marty, B., 1999. Heavy nitrogen in carbonatites of the Kola Peninsula: A possible signature of the deep mantle. *Science* (80-
844). 286, 2488–2490.

845 Elkins, L.J., Fischer, T.P., Hilton, D.R., Sharp, Z.D., McKnight, S., Walker, J., 2006. Tracing nitrogen in volcanic and geothermal volatiles from
846 the Nicaraguan volcanic front. *Geochim. Cosmochim. Acta* 70, 5215–5235.

847 Fischer, T.P., Giggenbach, W.F., Sano, Y., Williams, S.N., 1998. Fluxes and sources of volatiles discharged from Kudryavy, a subduction zone
848 volcano, Kurile Islands. *Earth Planet. Sci. Lett.* 160, 81–96.

849 Fischer, T.P., Hilton, D.R., Zimmer, M.M., Shaw, A.M., Sharp, Z.D., Walker, J.A., 2002. Subduction and recycling of nitrogen along the Central
850 American margin. *Science* (80-). 297, 1154–1157.

851 Fischer, T.P., Ramírez, C., Mora-Amador, R.A., Hilton, D.R., Barnes, J.D., Sharp, Z.D., Le Brun, M., de Moor, J.M., Barry, P.H., Füre, E., Shaw,
852 A.M., 2015. Temporal variations in fumarole gas chemistry at Poás volcano, Costa Rica. *J. Volcanol. Geotherm. Res.* 294, 56–70.
853 <https://doi.org/10.1016/j.jvolgeores.2015.02.002>

854 Füre, E., Hilton, D.R., Halldórsson, S.A., Barry, P.H., Hahm, D., Fischer, T.P., Grönvold, K., 2010. Apparent decoupling of the He and Ne
855 isotope systematics of the Icelandic mantle: The role of He depletion, melt mixing, degassing fractionation and air interaction.
856 *Geochim. Cosmochim. Acta* 74, 3307–3332. <https://doi.org/10.1016/j.gca.2010.03.023>

857 Füre, E., Marty, B., 2015. Nitrogen isotope variations in the Solar System. *Nat. Geosci.* 8, 515–522. <https://doi.org/10.1038/ngeo2451>

858 Füre, E., Portnyagin, M., Mironov, N., Deligny, C., Gurenko, A., Botcharnikov, R., Holtz, F., 2021. In situ quantification of the nitrogen content
859 of olivine-hosted melt inclusions from Klyuchevskoy volcano (Kamchatka): Implications for nitrogen recycling at subduction
860 zones. *Chem. Geol.* 120456.

861 Giggenbach, W.F., 1992. The composition of gases in geothermal and volcanic systems as a function of tectonic-setting, in: *International
862 Symposium on Water-Rock Interaction*. pp. 873–878.

863 Grady, M.M., Wright, I.P., Carr, L.P., Pillinger, C.T., 1986. Compositional differences in enstatite chondrites based on carbon and nitrogen
864 stable isotope measurements. *Geochim. Cosmochim. Acta* 50, 2799–2813.

865 Hashizume, K., Chaussidon, M., Marty, B., Robert, F., 2000. Solar wind record on the Moon: deciphering presolar from planetary nitrogen.
866 *Science* (80-.). 290, 1142–1145.

867 Henkes, G.A., Passey, B.H., Grossman, E.L., Shenton, B.J., Yancey, T.E., Pérez-Huerta, A., 2018. Temperature evolution and the oxygen
868 isotope composition of Phanerozoic oceans from carbonate clumped isotope thermometry. *Earth Planet. Sci. Lett.* 490, 40–50.

869 Hilton, D.R., Fischer, T.P., Marty, B., 2002. Noble gases and volatile recycling at subduction zones. *Rev. Mineral. geochemistry* 47, 319–
870 370.

871 Jackson, C.R.M., Cottrell, E., Andrews, B., 2021. Warm and oxidizing slabs limit ingassing efficiency of nitrogen to the mantle. *Earth Planet.
872 Sci. Lett.* 553, 116615.

873 Jackson, M.G., Blichert-Toft, J., Halldórsson, S.A., Mundl-Petermeier, A., Bizimis, M., Kurz, M.D., Price, A.A., Harðardóttir, S., Willhite, L.N.,
874 Breddam, K., 2020. Ancient helium and tungsten isotopic signatures preserved in mantle domains least modified by crustal
875 recycling. *Proc. Natl. Acad. Sci.* 117, 30993–31001.

876 Jambon, A., 1994. Earth degassing and large-scale geochemical cycling of volatile elements. *Volatiles in magmas* 479–518.

877 Javoy, M., 1998. The birth of the Earth's atmosphere: the behaviour and fate of its major elements. *Chem. Geol.* 147, 11–25.

878 Javoy, M., Pineau, F., 1991. The volatiles record of a “popping” rock from the Mid-Atlantic Ridge at 14°N: chemical and isotopic
879 composition of gas trapped in the vesicles. *Earth Planet. Sci. Lett.* 107, 598–611.

880 Labidi, J., Barry, P.H., Bekaert, D. V, Broadley, M.W., Marty, B., Giunta, T., Warr, O., Lollar, B.S., Fischer, T.P., Avice, G., 2020. Hydrothermal
881 ^{15}N ^{15}N abundances constrain the origins of mantle nitrogen. *Nature* 580, 367–371.

882 Labidi, J., Young, E.D., Fischer, T.P., Barry, P.H., Ballentine, C.J., de Moor, J.M., 2021. Recycling of nitrogen and light noble gases in the
883 Central American subduction zone: constraints from ^{15}N ^{15}N . *Earth Planet. Sci. Lett.*

884 Lee, H., Sharp, Z.D., Fischer, T.P., 2015. Kinetic nitrogen isotope fractionation between air and dissolved N_2 in water: Implications for
885 hydrothermal systems. *Geochem. J.* 49, 571–573.

886 Li, L., Bebout, G.E., 2005. Carbon and nitrogen geochemistry of sediments in the Central American convergent margin: Insights regarding
887 subduction input fluxes, diagenesis, and paleoproductivity. *J. Geophys. Res. Solid Earth* 110.

888 Li, L., Li, K., Giunta, T., Warr, O., Labidi, J., Lollar, B.S., 2021. N_2 in deep subsurface fracture fluids of the Canadian Shield: Source and

889 possible recycling processes. *Chem. Geol.* 120571.

890 Mallik, A., Li, Y., Wiedenbeck, M., 2018. Nitrogen evolution within the Earth's atmosphere–mantle system assessed by recycling in
891 subduction zones. *Earth Planet. Sci. Lett.* 482, 556–566.

892 Marty, B., 1995. Nitrogen content of the mantle inferred from N₂–Ar correlation in oceanic basalts. *Nature* 377, 326.

893 Marty, B., Chaussidon, M., Wiens, R.C., Jurewicz, A.J.G., Burnett, D.S., 2011. A 15N-poor isotopic composition for the Solar System as shown
894 by Genesis solar wind samples. *Science* (80-.). 332, 1533–1536.

895 Marty, B., Dauphas, N., 2003. The nitrogen record of crust–mantle interaction and mantle convection from Archean to Present. *Earth
896 Planet. Sci. Lett.* 206, 397–410. [https://doi.org/10.1016/s0012-821x\(02\)01108-1](https://doi.org/10.1016/s0012-821x(02)01108-1)

897 Marty, B., Gunnlaugsson, E., Jambon, A., Oskarsson, N., Ozima, M., Pineau, F., Torssander, P., 1991. Gas geochemistry of geothermal fluids,
898 the Hengill area, southwest rift zone of Iceland. *Chem. Geol.* 91, 207–225.

899 Marty, B., Humbert, F., 1997. Nitrogen and argon isotopes in oceanic basalts. *Earth Planet. Sci. Lett.* 152, 101–112.

900 Marty, B., Zimmermann, L., 1999. Volatiles (He, C, N, Ar) in mid-ocean ridge basalts: Assessment of shallow-level fractionation and
901 characterization of source composition. *Geochim. Cosmochim. Acta* 63, 3619–3633.

902 Marty, B., Zimmermann, L., Pujol, M., Burgess, R., Philippot, P., 2013. Nitrogen Isotopic Composition and Density of the Archean
903 Atmosphere. *Science* (80-.). 342, 101–104. <https://doi.org/10.1126/science.1240971>

904 Moreira, M., 2013. Noble gas constraints on the origin and evolution of Earth's volatiles. *Geochemical Perspect.* 2, 229–230.

905 Moreira, M., Kunz, J., Allegre, C., 1998. Rare gas systematics in popping rock: isotopic and elemental compositions in the upper mantle.
906 *Science* (80-.). 279, 1178–1181.

907 Moreira, M., Raquin, A., 2007. The origin of rare gases on Earth: The noble gas 'subduction barrier' revisited. *Comptes Rendus Geosci.* 339,
908 937–945.

909 Mukhopadhyay, S., 2012. Early differentiation and volatile accretion recorded in deep-mantle neon and xenon. *Nature* 486, 101–104.
910 <https://doi.org/10.1038/nature11141>

911 Parai, R., Mukhopadhyay, S., 2018. Xenon isotopic constraints on the history of volatile recycling into the mantle. *Nature* 560, 223.

912 Parai, R., Mukhopadhyay, S., Tucker, J.M., Pető, M.K., 2019. The emerging portrait of an ancient, heterogeneous and continuously evolving
913 mantle plume source. *Lithos* 346, 105153.

914 Pedroni, A., Hammerschmidt, K., Friedrichsen, H., 1999. He, Ne, Ar, and C isotope systematics of geothermal emanations in the Lesser
915 Antilles Islands Arc. *Geochim. Cosmochim. Acta* 63, 515–532.

916 Pinti, D.L., Hashizume, K., Matsuda, J., 2001. Nitrogen and argon signatures in 3.8 to 2.8 Ga metasediments: Clues on the chemical state of
917 the Archean ocean and the deep biosphere. *Geochim. Cosmochim. Acta* 65, 2301–2315.

918 Porcelli, D., Ballentine, C.J., Wieler, R., 2002. An Overview of Noble Gas Geochemistry and Cosmochemistry. *Rev. Mineral. geochemistry*
919 47, 1–19. <https://doi.org/10.2138/rmg.2002.47.1>

920 Roulleau, E., Sano, Y., Takahata, N., Kawagucci, S., Takahashi, H., 2013. He, N and C isotopes and fluxes in Aira caldera: comparative study
921 of hydrothermal activity in Sakurajima volcano and Wakamiko crater, Kyushu, Japan. *J. Volcanol. Geotherm. Res.* 258, 163–175.

922 Sano, Y., Fischer, T.P., 2013. The analysis and interpretation of noble gases in modern hydrothermal systems, in: *The Noble Gases as
923 Geochemical Tracers.* Springer, pp. 249–317.

924 Sano, Y., Takahata, N., Nishio, Y., Fischer, T.P., Williams, S.N., 2001. Volcanic flux of nitrogen from the Earth. *Chem. Geol.* 171, 263–271.

925 Sano, Y., Takahata, N., Nishio, Y., Marty, B., 1998. Nitrogen recycling in subduction zones. *Geophys. Res. Lett.* 25, 2289–2292.

926 Sano, Y., Urabe, A., Wakita, H., Chiba, H., Sakai, H., 1985. Chemical and isotopic compositions of gases in geothermal fluids in Iceland.

927 *Geochem. J.* 19, 135–148.

928 Snyder, G., Poreda, R., Hunt, A., Fehn, U., 2001. Regional variations in volatile composition: Isotopic evidence for carbonate recycling in

929 the Central American volcanic arc. *Geochemistry, Geophys. Geosystems* 2.

930 Staudacher, T., Allègre, C.J., 1988. Recycling of oceanic crust and sediments: the noble gas subduction barrier. *Earth Planet. Sci. Lett.* 89,

931 173–183.

932 Taenzer, L., Labidi, J., Masterson, A.L., Feng, X., Rumble III, D., Young, E.D., Leavitt, W.D., 2020. Low $\Delta^{12}\text{CH}_2\text{D}_2$ values in microbialgenic

933 methane result from combinatorial isotope effects. *Geochim. Cosmochim. Acta* 285, 225–236.

934 Taran, Y.A., 2011. N₂, Ar, and He as a tool for discriminating sources of volcanic fluids with application to Vulcano, Italy. *Bull. Volcanol.*

935 73, 395–408.

936 Taran, Y.A., 2009. Geochemistry of volcanic and hydrothermal fluids and volatile budget of the Kamchatka–Kuril subduction zone.

937 *Geochim. Cosmochim. Acta* 73, 1067–1094.

938 Trieloff, M., Kunz, J., Clague, D.A., Harrison, D., Allègre, C.J., 2000. The nature of pristine noble gases in mantle plumes. *Science* (80-.). 288,

939 1036–1038.

940 Vaselli, O., Tassi, F., Minissale, A., Montegrossi, G., Duarte, E., Fernandez, E., Bergamaschi, F., 2003. Fumarole migration and fluid

941 geochemistry at Poás volcano (Costa Rica) from 1998 to 2001. *Geol. Soc. London, Spec. Publ.* 213, 247–262.

942 Williams, C.D., Mukhopadhyay, S., 2018. Capture of nebular gases during Earth’s accretion is preserved in deep-mantle neon. *Nature* 565,

943 78–81. <https://doi.org/10.1038/s41586-018-0771-1>

944 Yeung, L.Y., 2016. Combinatorial effects on clumped isotopes and their significance in biogeochemistry. *Geochim. Cosmochim. Acta* 172,

945 22–38.

946 Yeung, L.Y., Ash, J.L., Young, E.D., 2015. Biological signatures in clumped isotopes of O₂. *Science* (80-.). 348, 431–434.

947 Yeung, L.Y., Li, S., Kohl, I.E., Haslun, J.A., Ostrom, N.E., Hu, H., Fischer, T.P., Schauble, E.A., Young, E.D., 2017. Extreme enrichment in

948 atmospheric ¹⁵N₁₅N. *Sci. Adv.* 3, eaao6741.

949 Young, E.D., Galy, A., Nagahara, H., 2002. Kinetic and equilibrium mass-dependent isotope fractionation laws in nature and their

950 geochemical and cosmochemical significance. *Geochim. Cosmochim. Acta* 66, 1095–1104.

951 Young, E.D., Kohl, I.E., Lollar, B.S., Etiope, G., Rumble Iii, D., Li, S., Haghnegahdar, M.A., Schauble, E.A., McCain, K.A., Foustoukos, D.I., 2017.

952 The relative abundances of resolved ¹²CH₂D₂ and ¹³CH₃D and mechanisms controlling isotopic bond ordering in abiotic and

953 biotic methane gases. *Geochim. Cosmochim. Acta* 203, 235–264.

954 Zimmer, M.M., Fischer, T.P., Hilton, D.R., Alvarado, G.E., Sharp, Z.D., Walker, J.A., 2004. Nitrogen systematics and gas fluxes of subduction

955 zones: insights from Costa Rica arc volatiles. *Geochemistry, Geophys. Geosystems* 5.

956

957

958

959

960

961

962

963